

CAI
FS 251
-80455



3 1761 11557732 2



**MANUSCRIPT
REPORT SERIES**

No. 55



Cotidal Charts for Canada

G. Godin

1980

Canada
Marine Sciences and Information Directorate
Department of Fisheries and Oceans
Ottawa, Ontario

A CLARIFICATION WITH REGARD TO MANUSCRIPT REPORT SERIES NO. 55

Page 21. (Line 10 from bottom)

Replace M_2 with S_2

Page 22. (Line 2 in legend)

Replace M_2 with S_2

Page 23. (The constants in the upper figure should read)

$$R = 3.2 \times 10^{-5} \text{ sec}^{-1} \quad x_0 = 340 \text{ km}$$

$$y_0 = -54 \text{ km}$$

(In the lower figure)

$$R = 5.5 \times 10^{-5} \text{ sec}^{-1} \quad x_0 = 344 \text{ km}$$

$$y_0 = -95 \text{ km}$$



Page 80. (Line 15 from bottom and Line 9 from bottom)

Replace 5 by 6

Page 89. (Line 10 from bottom)

Replace 5 by 6.



Digitized by the Internet Archive
in 2022 with funding from
University of Toronto

<https://archive.org/details/31761115577322>

Manuscript Report Series

No. 55

COTIDAL CHARTS FOR CANADA

G. Godin

1980

Marine Sciences and Information Directorate

Department of Fisheries and Oceans

Ottawa, Ontario K1A 0E6



Place names in Canada on a Miller projection.

CONTENTS

1. AVANT PROPOS - FOREWORD	4
2. COTIDAL CHARTS	5
2.1 Geographic chart	6
3. HARMONIC CONSTITUENTS: AMPLITUDE AND PHASE	6
4. PERIODIC WAVE MOTION.	9
4.1 One-dimensional motion (no rotation)	10
4.1.1 No friction	10
4.1.1.1 Progressive waves.	10
4.1.1.2 Standing waves	13
4.1.2 Wavelengths of tidal waves.	14
4.1.3 Construction of cotidal charts from	16
mathematical models	
4.1.4 One-dimensional standing wave motion.	17
with friction	
4.2 Two-dimensional motion with rotation and friction.	18
5. TIDAL PATTERNS.	25
6. COMMENTS ON THE COTIDAL CHARTS.	30
6.1 Charts for Canada.	32
6.1.1 Nodes and antinodes	32
6.1.2 Areas in need of further exploration.	41
6.2 Patterns of tides.	41
7. LARGE SCALE MAPS.	42
7.1 British Columbia	42
7.2 Gulf of St. Lawrence, Cape Breton and Newfoundland	54
7.3 Bay of Fundy	74
8. USE OF COTIDAL CHARTS FOR PREDICTION.	74
9. ACKNOWLEDGMENTS	81
10. REFERENCES.	90
11. FIGURE CAPTIONS	91

1. AVANT-PROPOS

Une carte cotidale est une extrapolation géographique de la phase et de l'amplitude d'une onde composante, obtenues par l'analyse harmonique de la marée observée en divers points de l'océan et consiste de courbes de phase et d'amplitude constantes. Elle sert à interpréter les données disponibles, à vérifier les résultats d'analyses subséquentes et à comprendre la dynamique des marées. Nous pouvons construire des cartes cotidales adéquates pour les eaux adjacentes au Canada que l'on peut interpréter à l'aide de la théorie élémentaire du mouvement ondulatoire dans un océan tournant. La théorie suggère l'existence de structures typiques telles que points d'amphidromie et ventres que l'on devrait retrouver dans la nature. Un jeu de cartes cotidales des ondes majeures peut servir aussi à préparer des prédictions approximatives de la marée pour tous les points des océans qu'il couvre.

On a accumulé systématiquement des données sur la marée au Canada depuis la fondation du Bureau des Levées de Marées par W.B. Dawson en 1894. L'Amirauté Anglaise avait fait auparavant des levées sporadiques dans la Baie de Fundy, le Golfe du Saint-Laurent, autour de Terre-Neuve, le long de notre côte du Pacifique et dans l'arctique. Depuis 1894 on a accumulé systématiquement les données et elles ont formé la base d'un grand nombre de travaux scientifiques et pratiques. Les cartes cotidales que je présente ici constituent une distillation et une interprétation du matériel très vaste qui est maintenant à notre disposition.

FOREWORD

Cotidal charts constitute a geographical extrapolation of the major harmonic constants obtained from a harmonic analysis of the tide observed at points in and around the ocean; they consist of contours of equal phase and equal amplitude. They are of value in interpreting the data available, for checking the results of further analyses and for understanding the dynamics of tidal motion. It is possible to draw fair cotidal charts for the waters adjacent to Canada which may be interpreted using the results of the theory of elementary wave motion in a rotating ocean. Such theory suggests structures which should be found in nature such as amphidromies and antinodes. A set of cotidal charts of the major harmonic constituents can also be used to make approximate predictions of the tide at any point of the oceans which they cover.

Tidal information about Canadian waters has been accumulated systematically since the establishment of the Tidal Survey with W.B. Dawson in 1894. Previously the British Admiralty had made sporadic measurements in the Bay of Fundy, the Gulf of St. Lawrence, around Newfoundland, on the Pacific west coast and in the arctic. Since 1894 the information has been systematically compiled and scrutinized to become the source material for numerous scientific and practical investigations. The cotidal charts which I present here constitute one such result; a distillation and interpretation of the very extensive material now available.

2. COTIDAL CHARTS

Cotidal charts provide a visual summary of available information about the major harmonic constituents of the vertical tide. If a plot is made on a geographic chart of the amplitude and phase of these constituents at the stations available, it is readily apparent that they vary smoothly from point to point and it is possible by simple extrapolation to draw contours over the water body. No theory is involved at this stage.

Elementary physical theory indicates that the tide is a long wave phenomenon. Harmonic constituents have a precise frequency and a basin of a given configuration will respond in a definite way to a forced oscillation: nodes and antinodes will be formed at specific locations. These should become apparent during the inspection of the data. The existence of a node is revealed by a rapid change of phase around a given point and a marked decrease in the amplitude there. An antinode is found in an area where the phase is virtually constant while the amplitude passes through a maximum. The end product of this task of interpretation, interpolation and extrapolation is a cotidal chart. The data are seldom dense enough to draw it unambiguously so that a cotidal chart contains a certain element of arbitrariness. Nevertheless, cotidal charts are useful tools in study of the tide and one should never hesitate to prepare one even if the information available appears sadly lacking.

In brief:

- 1) Cotidal charts help summarize the information presently available on the tide in a given area.
- 2) They may be used to check the results of analyses of short sets of observations at temporary gauging sites; gross errors in the recordings or in time keeping may be picked up by plotting the analyzed values on the appropriate charts. They also form the basis for more precise and plausible sets of cotidal charts when additional information becomes available.
- 3) They help in pointing areas where the tidal coverage is inadequate and where further exploration is necessary. Canadian waters are extensive and only by careful planning and systematic execution will it ever be possible to obtain a general understanding of the tide in our waters.
- 4) Wherever the tide has a good semidiurnal character (this will be defined more precisely further on), the M_2 chart alone suffices to give a good estimate of the mean amplitude of the tide at a given site (the range is twice the amplitude) and of the mean time of high and low water.
- 5) A correctly drawn cotidal chart reveals the structure of the tidal wave of the given frequency in the basin under consideration and helps stimulate a search for a theoretical confirmation of the assumed structures.
- 6) Cotidal charts may be used to predict the tide in the particular area.
- 7) Cotidal charts help control the results of numerical modelling of the tide in the ocean.

2.1 Geographic chart

I have used a Miller projection as a background geographic chart (frontispiece). This is an intermediate cylindrical projection. The meridians as well as the parallels are straight parallel lines which have been devised for better representation of high latitude regions. The parallels are spaced much closer than on Mercator's to reduce excessive latitudinal expansion, and farther apart than on the Lambert Equal-Area Cylindrical, to avoid extreme polar flattening.

No projection can display perfectly on a plane a large portion of the earth's sphere; the Miller projection in particular gives more emphasis to northern areas, and since we have much more exploratory work to do in our northern regions its use helps emphasize where more measurements are required. In any case the southern regions where more measurements are available are presented here in larger scale.

3. HARMONIC CONSTITUENTS: AMPLITUDE AND PHASE

The vertical tide $z(t)$ may be adequately represented by the expression:

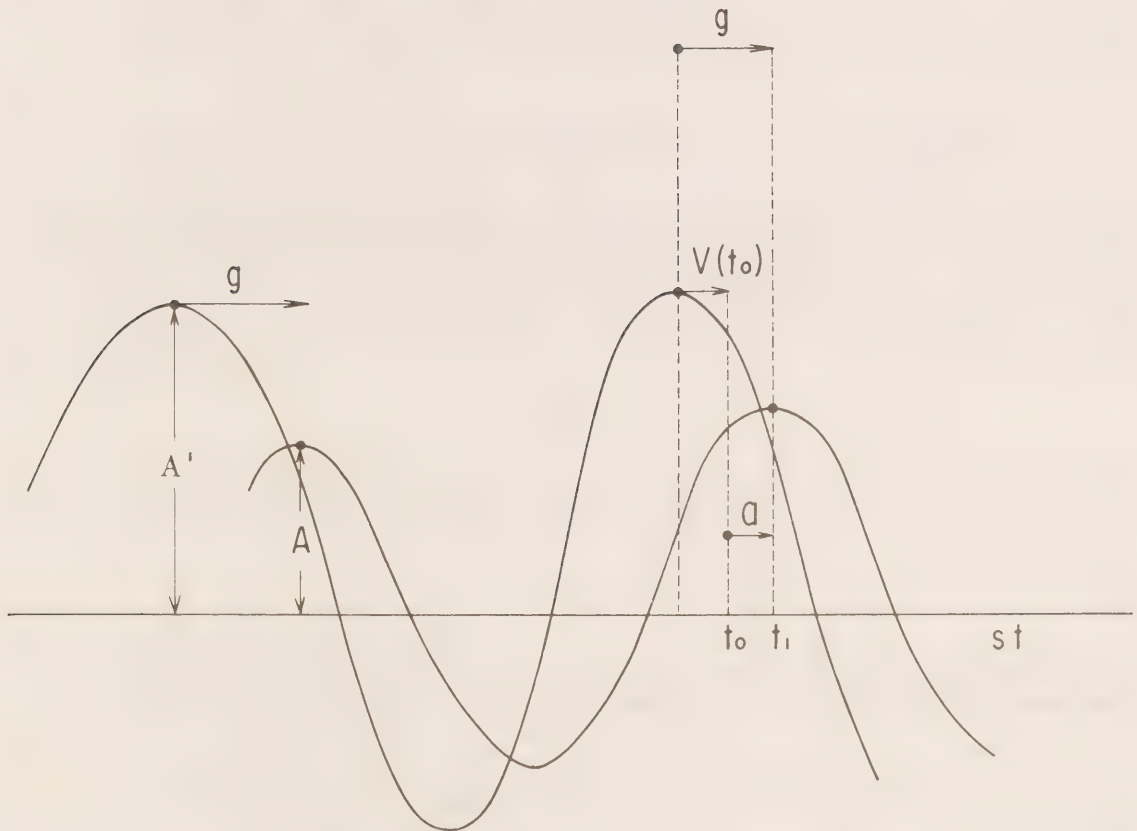
$$z(t) = z_0 + \sum_{j=1}^n A_j \cos(\sigma_j t - a_j) \quad (1)$$

where z_0 is a constant which denotes the reference level, which in oceanography represents the mean sea level (whenever this quantity can be adequately defined and calculated); on navigational charts z_0 is an arbitrary elevation chosen in such a way that the observed water level seldom falls below it. The second term is a superposition of n pure harmonics of amplitude A , frequency σ and phase a ; it represents the tide proper. (1) Indicates that at most places the tide may be represented by a sum of sinusoids of known frequencies, but whose amplitudes and phases are characteristic of the site. A harmonic analysis determines the amplitude and the phase of each harmonic component (constituent) from observations on the local variations of water level. The number n of such constituents is very large (over 500); in practice a handful of harmonics in the diurnal and semidiurnal bands is much larger than the others combined and suffice to give a good approximation to the tide. These are given in Table 1. Other constituents such as μ_2 , ν_2 and L_2 also contribute significantly to the tide, but as their resolution and interpretation are more difficult we exclude them from the set of charts we wish to present. We also exclude the charts of P_1 and K_2 , because these constituents have frequencies close to K_1 and S_2 respectively.

The contribution of a given constituent to the local tide is, as already said, a pure sinusoid of amplitude A and phase a which we illustrate in Figure 1. We have found it preferable to replace the time scale t by the phase change σt which enters in (1). We notice immediately that the phase a will vary with each time origin t_0 chosen for a specific analysis. This is a source of confusion and an accepted convention in tidal analysis is to

Table 1. Frequency of the major tidal constituents.

Diurnal band		Semidiurnal band	
Constituent	Frequency (deg/h)	Constituent	Frequency (deg/h)
O_1	13.94	N_2	28.44
P_1	14.96	M_2	28.98
K_1	15.04	S_2	30.00
		K_2	30.08

Fig. 1. Relation between the local constituent $A \cos (\sigma t-a)$ and the corresponding component of the tidal force $A' \cos V(t)$.

replace the phase lag a by the Greenwich phase lag g which is defined in the following way. The phase of the component of the tidal force corresponding to the specific constituent can be calculated from known astronomical data; it is called $V(t)$, the "astronomical argument" and it has value $V(t_0)$ at the chosen time origin for the analysis. $V(t_0)$ is calculated routinely in the course of a harmonic analysis. The Greenwich phase lag g is defined by the expression:

$$-a \equiv V(t_0) - g \quad (2)$$

or better;

$$g \equiv V(t_0) + a \quad (3)$$

Figure 1 illustrates the meaning of g : it is the phase lag between the instant the component in the tidal force reaches its peak and the instant of maximum contribution of the constituent to the local vertical tide. Physically it is the delay between the time a force is applied and the time it causes maximum deformation. The phase lag g has the same value for any choice of the time origin t_0 . However the value of g also depends on the time zone Z used to determine the time of the culmination of the component tidal displacement; in order to resolve this ambiguity, all the phase lags g in the charts presented have been calculated for the Greenwich time zone

$$Z = 0,$$

so that the g 's contoured in the charts are directly comparable from one site to the other. The translation of the Greenwich phase lag for a local time zone $Z = r$ is given by the formula:

$$g_r = g - r \sigma \quad (4)$$

As an example the Greenwich phase lag for K_1 at Victoria is:

$$g = 269.2^\circ$$

Since Victoria lies in time zone $Z = +8$, the Greenwich phase lag for K_1 (frequency $15.04^\circ/\text{h}$) in local time is:

$$g_8 = 269.2 - 8 \times 15.04 = 148.9^\circ$$

The amplitude A of the constituent is independent of the time scale and of z_0 the level of reference used. The value A and g of the constituents at the gauging stations where the tide was observed form the source material of

the cotidal charts.

4. PERIODIC WAVE MOTION

It is useful in the preparation of cotidal charts to have some understanding of periodic wave motion in a basin, which understanding, in turn, can only be obtained with the help of a formal solution of the linearized equations of hydrodynamics. In rectangular components these have the form, taking account of the rotation of the earth and of friction:

$$\frac{\partial u}{\partial t} - fv = -g \frac{\partial Z}{\partial x} - ru \quad (5)$$

$$\frac{\partial v}{\partial t} + fu = -g \frac{\partial Z}{\partial y} - rv \quad (6)$$

$$H \left(\frac{\partial u}{\partial x} + \frac{\partial v}{\partial y} \right) + \frac{\partial Z}{\partial t} = 0 \quad (7)$$

where u , v are the east and north components of the current vectors; Z is the vertical displacement of the surface; $f = 2\Omega \sin \phi$ (in which Ω is the speed of rotation of the earth and ϕ the latitude) is the Coriolis coefficient; g is the acceleration due to gravity; H the depth (assumed constant) and r is the linearized coefficient of friction. Motion is presumed two-dimensional and homogeneous in the vertical (barotropic); (x, y) denotes the coordinates of the point of measurement in flat space and t the time variable. For periodic motion (the case of the tide), the time variation of u , v and Z can be represented by:

$$u, v, Z \sim e^{i\sigma t}$$

so that $\frac{\partial}{\partial t}$ becomes $i\sigma$ and (5), (6) and (7) take the form:

$$(i\sigma + r) u - fv = -g \frac{\partial Z}{\partial x} \quad (8)$$

$$fu + (i\sigma + r) v = -g \frac{\partial Z}{\partial y} \quad (9)$$

$$H \left(\frac{\partial u}{\partial x} + \frac{\partial v}{\partial y} \right) = -i\sigma Z \quad (10)$$

(8) to (10) form a set of linear first-order differential equations in the unknowns u , v and Z defined over a basin whose dimensions are specified for each problem to be solved. In the present study we presume that the basin is rectangular. Their solution in a finite domain consists of Kelvin and Poincaré waves that can be combined linearly in order to satisfy specific boundary conditions. In spite of the ready availability of complete and exact solutions of (8), (9) and (10), they are so involved that it is preferable to work toward them in stages of increasing physical complication. I begin with one-dimensional motion.

4.1 One dimensional motion (no rotation)

4.1.1 No friction

Equations (8), (9) and (10) reduce to:

$$i\sigma u = -g \frac{\partial Z}{\partial x} \quad (11)$$

$$H \frac{\partial u}{\partial x} = -i\sigma Z \quad (12)$$

where we made $v = f = r = 0$ and the basin becomes a canal. The solution of (11), (12) with the time variation is:

$$Z = (Ae^{ikx} + B e^{-ikx}) e^{i\sigma t} \quad (13)$$

$$u = -\sqrt{\frac{g}{H}} (Ae^{ikx} - B e^{-ikx}) e^{i\sigma t} \quad (14)$$

where k , the wave number, stands for σ/\sqrt{gH} . A and B are arbitrary constants of integration to be determined from the boundary conditions. The physically significant part of the solution is the real part of the expressions for Z and u . We note that:

$$e^{ia} = \cos a + i \sin a \quad (15)$$

where a is usually expressed in radians and is dimensionless.

4.1.1.1 Progressive waves

If the boundary condition is such that:

$$A = 0 \quad \text{or} \quad B = 0$$

the solution (13), (14) reduces to:

$$Z_1 = B e^{i(\sigma t - kx)} \quad \text{or} \quad Z_2 = A e^{i(\sigma t + kx)}$$

$$u_1 = B \sqrt{\frac{g}{H}} e^{i(\sigma t - kx)} \quad u_2 = -A \sqrt{\frac{g}{H}} e^{i(\sigma t + kx)}$$

which, in real form, assuming A and B real, become:

$$Z_1 = B \cos (\sigma t - kx) \quad (16) \quad Z_2 = A \cos (\sigma t + kx) \quad (18)$$

$$u_1 = B \sqrt{\frac{g}{H}} \cos (\sigma t - kx) \quad (17) \quad u_2 = -A \sqrt{\frac{g}{H}} \cos (\sigma t + kx) \quad (19)$$

These solutions represent oscillatory waves travelling in the direction of increasing or decreasing x . In order to visualize this we study the profile of the elevation and the current along the canal (Figure 2a) between $kx = 0$ and $kx = 360^\circ$ for various time steps for the solution (16) and (17). The heavy line in the surface represents its displacement with respect to its equilibrium position. The arrows denote the direction and intensity of the associated current; a dot indicates a position of null current. The four consecutive figures for times corresponding to 0° to 270° of phase indicate that the surface appears to be affected by a wave travelling from left to right. The associated currents are null at the nodes, positive and maxima at the crests, and negative and minima at the troughs. The second solution would represent a wave travelling from right to left with the same velocity.

The wavelength L is obtained from:

$$Z(x_0 + L) = Z(x_0) \quad \text{or} \quad \cos (\sigma t - k(x_0 + L)) = \cos (\sigma t - kx_0)$$

which implies

$$kL = 2\pi \quad \text{or} \quad L = \frac{2\pi}{k}$$

The period T of the wave is determined from the condition:

$$Z(t+T) = Z(t) \quad \text{or} \quad \cos (\sigma[t+T] - kx) = \cos (\sigma t - kx)$$

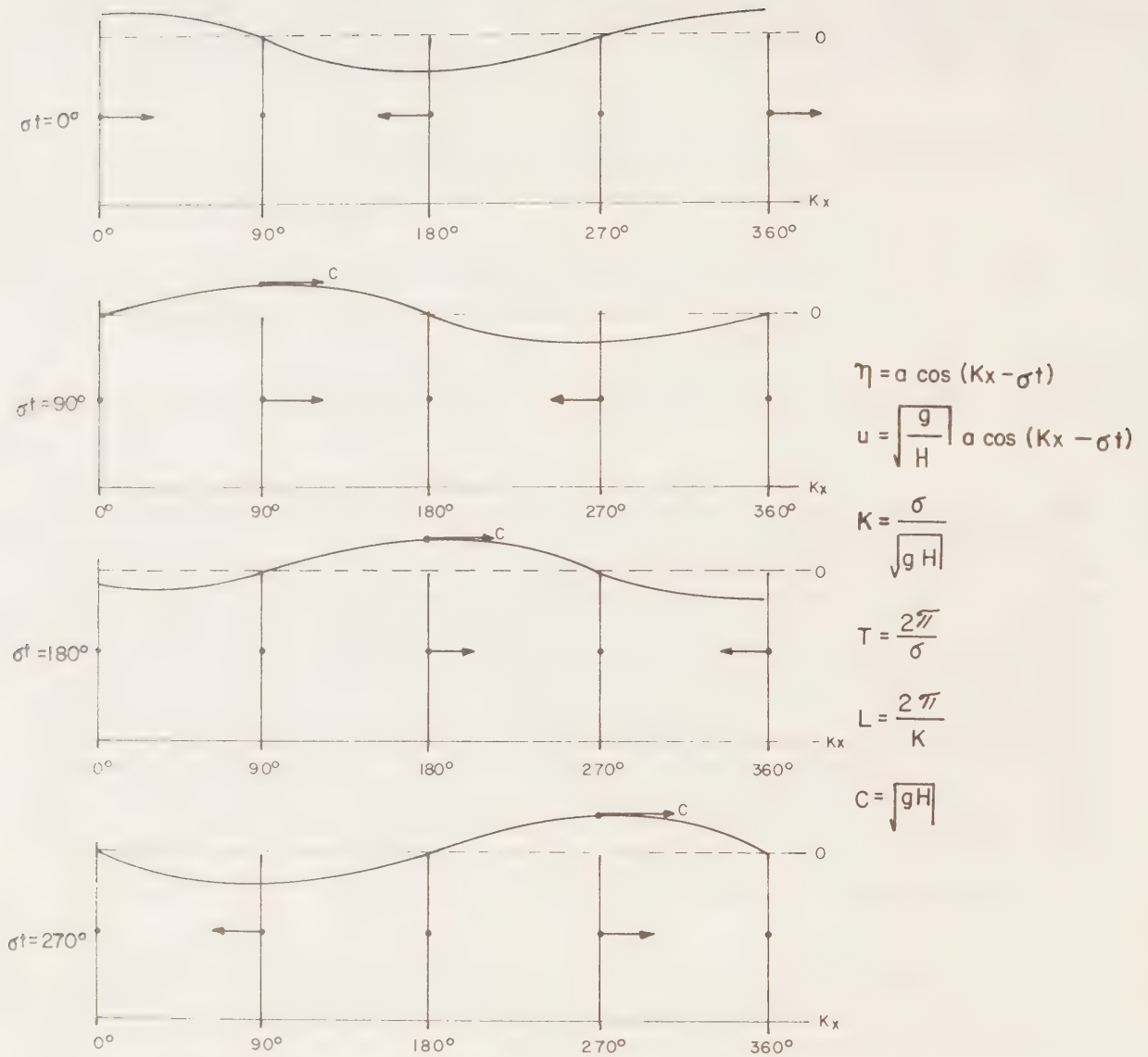


Fig. 2a. Profile of the surface of a fluid in a canal and corresponding horizontal velocities at various times when it is disturbed by a travelling wave.

which implies

$$T = \frac{2\pi}{\sigma}$$

Finally the velocity c of displacement of the crest is obtained from the condition:

$$\frac{d}{dt}(\sigma t - kx) = 0 \quad \text{or} \quad \sigma = k \frac{dx}{dt} = kc$$

Therefore:

$$c = \sqrt{gH}$$

The second solution gives a wave with the same wavelength, period and velocity, but with displacements in the opposite direction.

4.1.1.2 Standing waves

If $A = B$ or if $A = -B$, the solution (13) (14) takes the special form:

$$Z_1 = A' \cos kx \cos \sigma t \quad (20) \quad Z_2 = A'' \sin kx \cos \sigma t \quad (22)$$

$$u_1 = A' \sqrt{\frac{g}{H}} \sin kx \cos (\sigma t - \pi/2) \quad (21) \quad u_2 = A'' \cos kx \cos (\sigma t + \pi/2) \quad (23)$$

$$\text{where} \quad A' \equiv 2A \quad A'' \equiv 2iA$$

These two special solutions represent standing waves. In (20) (21) the current u vanishes at:

$$x = 0$$

This point can be considered as the position of a wall against which a wave travelling from the right is perfectly reflected to return to the right without any change in amplitude. This interpretation can be supported algebraically noting that:

$$Z_1 = A' \cos kx \cos \sigma t = \underbrace{A \cos (\sigma t + kx)}_{\substack{\text{(wave travelling} \\ \text{from the right)}}} + \underbrace{A \cos (\sigma t - kx)}_{\substack{\text{(wave travelling} \\ \text{to the right)}}} = 2A \cos \sigma t \cos kx$$

The second solution also represents a standing wave with perfect reflexion at $kx = \pi/2$. In a standing wave the water level oscillates vertically without apparent displacement of the wave crest. The associated current is maximum at the points where the amplitude of the vertical displacement is zero and vice versa. The wavelength is still:

$$L = 2\pi/k \quad \text{and the period is still} \quad T = 2\pi/\sigma,$$

but the velocity of displacement is 0 (Figure 2b). Standing and travelling waves represent extreme cases of periodic motion in one dimension. Any intermediate type of motion can be considered as a superposition of two travelling or two standing waves with different amplitude and phase.

Tidal motion in the ocean and in neighbouring basins has a standing wave character and we will be able to interpret the cotidal charts by representing the motion by a solution of the form (20) (21) modified for the effect of the earth's rotation and of friction.

4.1.2 Wavelengths of tidal waves

The cotidal charts are presented for the constituents O_1 , K_1 , N_2 , M_2 and S_2 . Their frequencies and associated periods are as shown (Table 2).

Table 2. Periods of the constituents considered in the cotidal charts.

Constituent	Frequency σ		Period T
	$^\circ/h$	radians/sec	
O_1	13.9430	$.676 \times 10^{-4}$	25.8
K_1	15.0411	$.729 \times 10^{-4}$	23.9
N_2	28.4397	1.379×10^{-4}	12.7
M_2	28.9841	1.405×10^{-4}	12.4
S_2	30.0000	1.454×10^{-4}	12.0

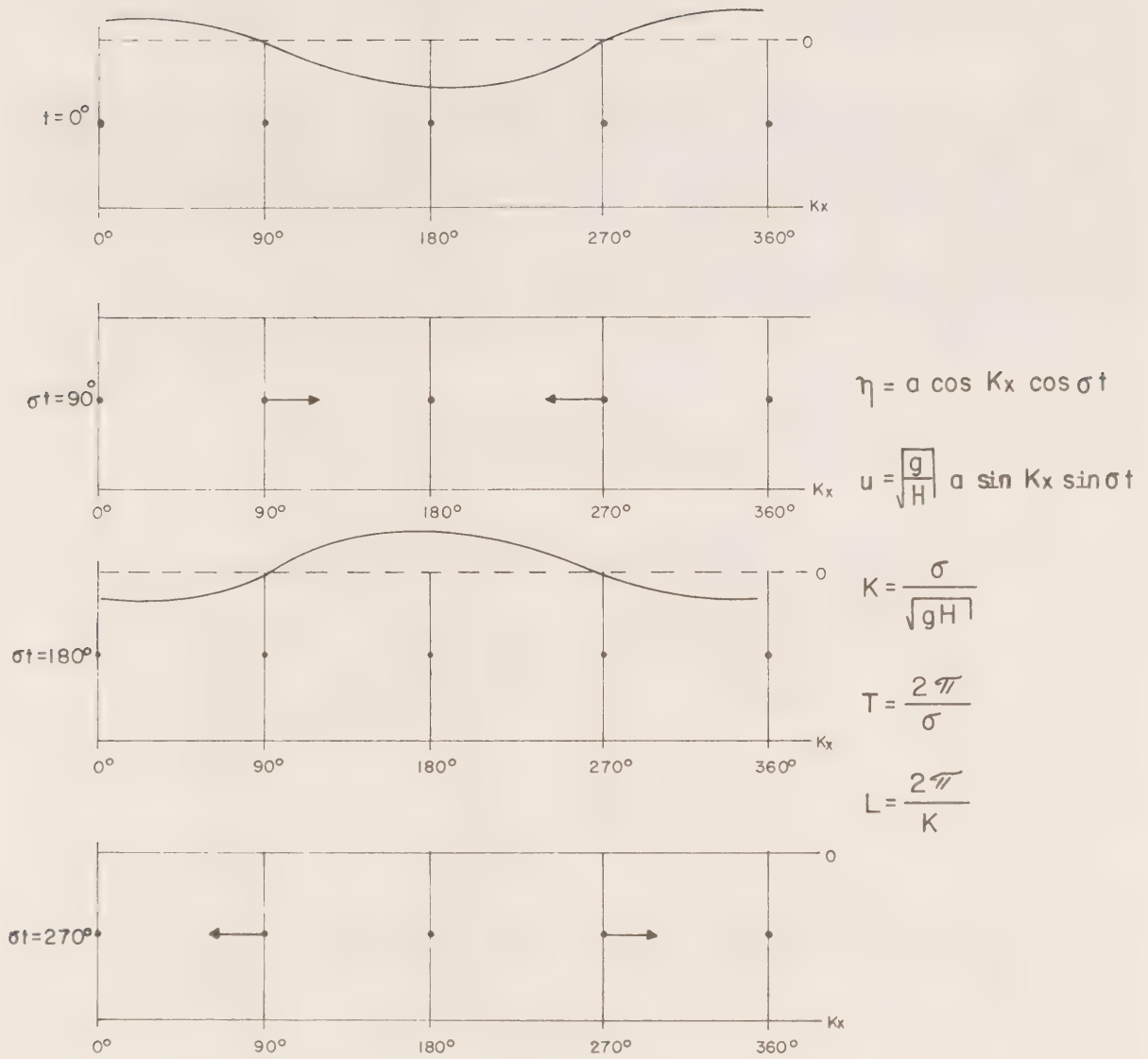


Fig. 2b. Profile of the surface of a fluid in a canal and corresponding horizontal velocities at various times when it is disturbed by a standing wave.

We calculate the wavelengths L and velocities c of the constituents M_2 and K_1 which predominate in the semidiurnal and diurnal bands for various values of the depth H (Table 3). Although tidal motion behaves as a standing wave, in general we still calculate the velocity c of a progressive wave. The reason is that the tide may assume the character of a travelling wave in narrow and shallow rivers; the effect of friction is such that the velocity of displacement of the tidal wave is less than the value indicated in the table.

The order of magnitude of the wavelength is more relevant to the interpretation of cotidal charts. The wavelength of the diurnal tide is twice that of the semidiurnal, so that the distance between diurnal nodes should be twice as large as between semidiurnal nodes. If we find a node, semidiurnal or diurnal, it provides a clue as to the location of the node of the other species. The distance between nodes of the same species should be half a wavelength (for a constant depth).

Table 3. Velocity and wavelength of the tidal waves associated with the constituents M_2 and K_1 .

Depth	Associated velocity for a free travelling wave	M_2 Wavelength	K_1 Wavelength
H m	$c = \sqrt{gH}$ km/h	$L=2\pi/k=Tc$ km	$L=Tc$ km
10	36	447	862
50	80	994	1915
100	113	1404	2705
500	252	3130	6031
1000	357	4435	8545
5000	797	9901	19076

4.1.3 Construction of cotidal charts from mathematical models

We wish to utilize the elementary theory developed above to draw cotidal charts corresponding to travelling or standing waves. A cotidal chart consists of the field of amplitudes and phase lags in the time dependent part of the solution, whether it be the elevation Z or the current u . In the solution for a travelling wave, i.e. (16) and (17), both Z and u have the same time dependence, kx being the phase lag; their amplitude differs by a constant factor $\sqrt{g/H}$. Here one cotidal chart suffices for both Z and u . The solution for a standing wave, (20) and (21), gives no phase lag for Z

but the amplitude is affected by the factor $\cos kx$; this factor determines areas where the amplitude is positive or negative. Since we keep the amplitude always positive in our charts, we treat a negative amplitude as consisting of a positive amplitude with a phase lag of 180° , i.e.:

$$-A \cos \sigma t = A \cos (\sigma t - 180^\circ)$$

In a canal, the point where $\cos kx = 0$ determines the node which takes the form of a line across it. The solution for the current indicates a constant phase lag of 90° with respect to the vertical tide, but the possible sign change of $\sin kx$ also brings an additional phase lag of 180° in the zones where $\sin kx$ is negative.

With these remarks we go on to search for a solution of a standing wave with friction and then will draw cotidal charts for all the cases studied in order to see their appearance and their modification by the introduction of additional effects.

4.1.4 One-dimensional standing wave motion with friction

In the case of one-dimensional motion with friction ($v = f = 0$) the equations have the form:

$$(i\sigma + r) u = -g \frac{\partial Z}{\partial x} \quad (25)$$

$$H \frac{\partial u}{\partial x} = -i\sigma Z \quad (26)$$

and the solution has the same form as (13) and (14) except that k is replaced by k' where:

$$k' = \frac{\sigma}{\sqrt{gH}} \sqrt{1 - ir/\sigma}$$

The form of this factor indicates that it is no longer an elementary matter to separate the real and imaginary terms in the solution; it is useful to retain the time dependence of the time in the form $e^{i\sigma t}$ until the very last stages of the calculations. Whatever complex factor is present in the solution it can always be written in form Re^{-1r} , where r is an added contribution to the phase lag.

The solution of (25) (26), which represents a standing wave with perfect reflexion at the origin ($u = 0$ at $x = 0$), is:

$$Z = A \cos k'x \cos \sigma t \quad (27)$$

$$u = A \sqrt{\frac{g}{H}} \frac{\sin k'x \cos (\sigma t - 1/2\pi)}{\sqrt{1 - ir/\sigma}} \quad (28)$$

where we have dropped the prime in A' . Since $k'x$ is a complex number, its cosine or sine consists in fact of products of trigonometric and hyperbolic functions. It follows then that the constant A is complex in general and this must be taken into account in the calculation of the effective phase lags of the elevation or of the current. The current satisfies the condition of perfect reflexion at $x = 0$ because $\sin k'x = 0$ for $x = 0$ even if k' is complex. On the other hand $\cos k'x$ has no zero whatsoever, which in turn indicates that there is no node possible for such type of motion. We call it a standing wave with perfect reflexion; it could be considered as well the superposition of two waves travelling in opposite directions, with the wave reflected from the wall having a smaller amplitude. We now draw cotidal charts for a travelling wave and a standing wave without friction and then another set for a standing wave with friction. We show only the chart for the elevation of a travelling wave.

The cotidal chart for the travelling wave (Figure 3a) shows a canal open at the origin; it contains only cophase lines which increase for increasing x . There are no coamplitude lines because the amplitude of the wave is uniform everywhere. In the second pair (Fig. 3b) of cotidal charts the canal is closed at $x = 0$. The charts are those of the vertical tide Z and the associated horizontal current u in a standing wave. Cophase and coamplitude lines coincide in many points; in this case the coamplitude is pulled out of the canal and the corresponding amplitude is written outside as well. In the vertical tide we get a maximum amplitude at the origin and at the position $kx = 180^\circ$. The node is at $kx = 90^\circ$ and it is marked by a coamplitude line of 0. The corresponding cotidal chart of the current shows that it has uniform phase between $x = 0$ and $kx = 180^\circ$ where the node of the current is to be found. It has maximum amplitude at the position of the node of the vertical tide. The other pair (Fig. 3c) of charts show the same standing wave, but this time affected by friction. The chart for the vertical tide shows that the node at $kx = 90^\circ$ has disappeared and has been replaced by a minimum of .2. The jump of 180° at the node is now replaced by a rapid change of 340 to 220° . Similarly for the current, the abrupt change in phase from 90° to 270° is replaced by a change from 70 to 10° in the vicinity of the node of the current. The latter charts are more physically reasonable. They show half a wavelength in a standing oscillation. Numerous observations are available on Z which permit us to verify such an hypothesis; whereas the few data on u forbid the elaboration of similar cotidal charts for the horizontal tide.

4.2 Two-dimensional motion with rotation and friction

The equations to solve are (8) to (10) and their general solution has

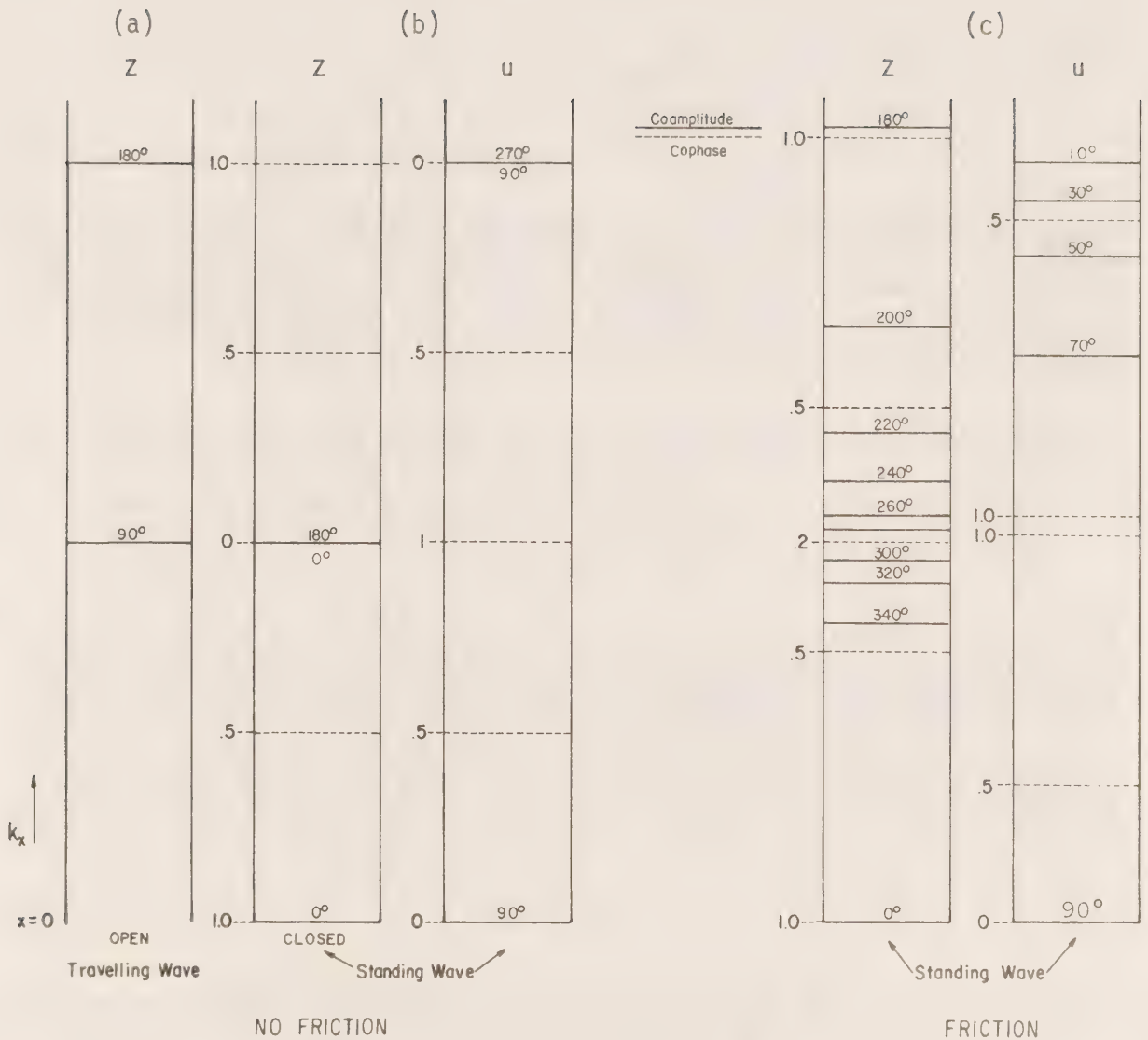


Fig. 3. Cotidal charts in a canal half a wavelength long (one-dimensional motion). Continuous line - cophase contour. Dashed line - coamplitude contour.

- a) Travelling wave: vertical displacement Z .
- b) Standing wave, no friction: vertical displacement Z and horizontal velocity u .
- c) Standing wave affected by friction: Z and u .

the form:

$$Z = (Ae^{ik_1x} + Be^{-ik_1x}) (Ce^{ik_2y} + De^{-ik_2y}) e^{i\sigma t} \quad (29)$$

where

$$k_1^2 + k_2^2 = \frac{(\sigma - ir)^2 - f^2}{gH}$$

k_1 , or k_2 , usually forms a set of eigenvalues whenever a boundary condition of zero velocity is imposed on the x or y boundary; the corresponding set of solutions is known as Poincaré waves. If k_1 (or k_2) is pure imaginary (this is determined by the width and depth of the sea), the Poincaré waves are damped rapidly away from the boundaries and are not significant over the body of the sea.

In addition to (29), the equations (8) to (10) also have a solution which satisfies:

$$v \equiv 0$$

throughout the domain; this is the Kelvin solution. It is the equivalent of that which we have been studying in one-dimension, but with the additional effect of rotation. It represents a very simple mode of motion and as we shall see, seems to be preferred by the ocean.

The Kelvin solution for (8) to (10) analogous to the one-dimensional solution (27) (28), is:

$$Z = A \cos (k'x - im'y) e^{i\sigma t} \quad (30)$$

$$u = A \sqrt{\frac{g}{H}} \frac{1}{\sqrt{1 - ir/\sigma}} \sin (k'x - im'y) e^{i(\sigma t - \pi/2)} \quad (31)$$

$$\text{where } k' = \frac{\sigma}{\sqrt{gH}} \sqrt{1 - ir/\sigma}, \quad m' = \frac{f}{\sqrt{gH}} \frac{1}{\sqrt{1 - ir/\sigma}} \quad \text{and where}$$

m' represents the distorting effect of rotation. The prime in both parameters k and m indicates that linearized friction is also taken into account.

We give (Fig. 4) schematic cotidal charts of the solutions (30) and (31) for the particular case of no friction ($r = 0$); they should be studied in comparison with those of one-dimensional standing wave with no friction.

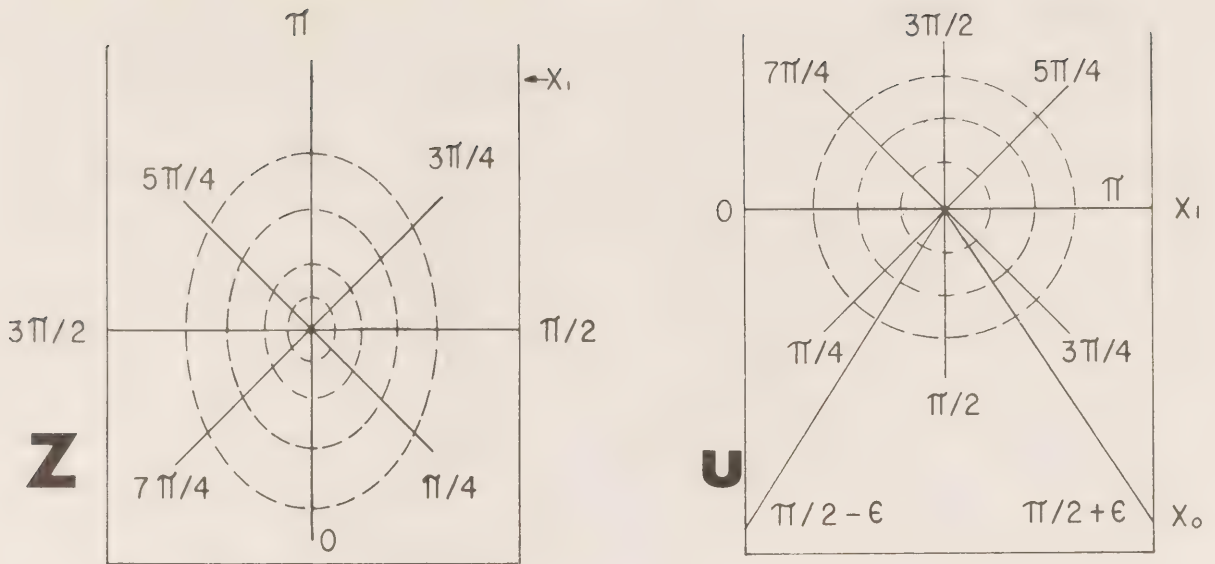


Fig. 4. Schematic cotidal charts for a standing Kelvin wave (no friction); they are the rotary counterpart of chart (b) in Fig. 3. The nodal line has been transformed into a point (amphidromy) by the rotation and the cophase lines now radiate from it. The node of the current (at x_1) corresponds to the antinode of the vertical displacement and vice versa.

The new chart of Z may be compared with the original one being rotated counterclockwise and we see that the nodal line is now a point (amphidromy). Along the central line of the basin the lines follow exactly the same progression as in one dimension. The same comparison can be made with the charts for the current u . We do not draw the charts as far as the boundary $x = 0$ in two-dimensions because the Kelvin solution is not the only one present near the boundary; an infinity of Poincaré waves also exists in that vicinity in order to ensure the satisfaction of the condition of zero flow all across the boundary at $x = 0$.

The diagrams given are valid for the northern hemisphere; the crest of high water rotates counterclockwise around the node. We notice that maximum currents are still found at the node of the vertical tide and vice versa. As already said, we have little opportunity in practice to verify the cotidal chart of the current u .

We give (Fig. 5) the cotidal charts for a standing Kelvin wave for various degrees of friction in a specific basin for the constituent M_2 and illustrate exclusively the vertical displacement Z given by the solution (30). The contours are in arbitrary units and are not directly comparable from the case of no friction to those with friction. They indicate qualitatively that along the canal the change in amplitude on the "left side" of the canal (with respect to the reflecting wall) becomes less marked for increasing values of the friction while on the "right side" the amplitudes pass through an increasingly deeper and more abrupt minimum. The gradual displacement of the node by increasing friction can be confirmed quantitatively by searching the position of the node of solution (30).

LATITUDE 45° N

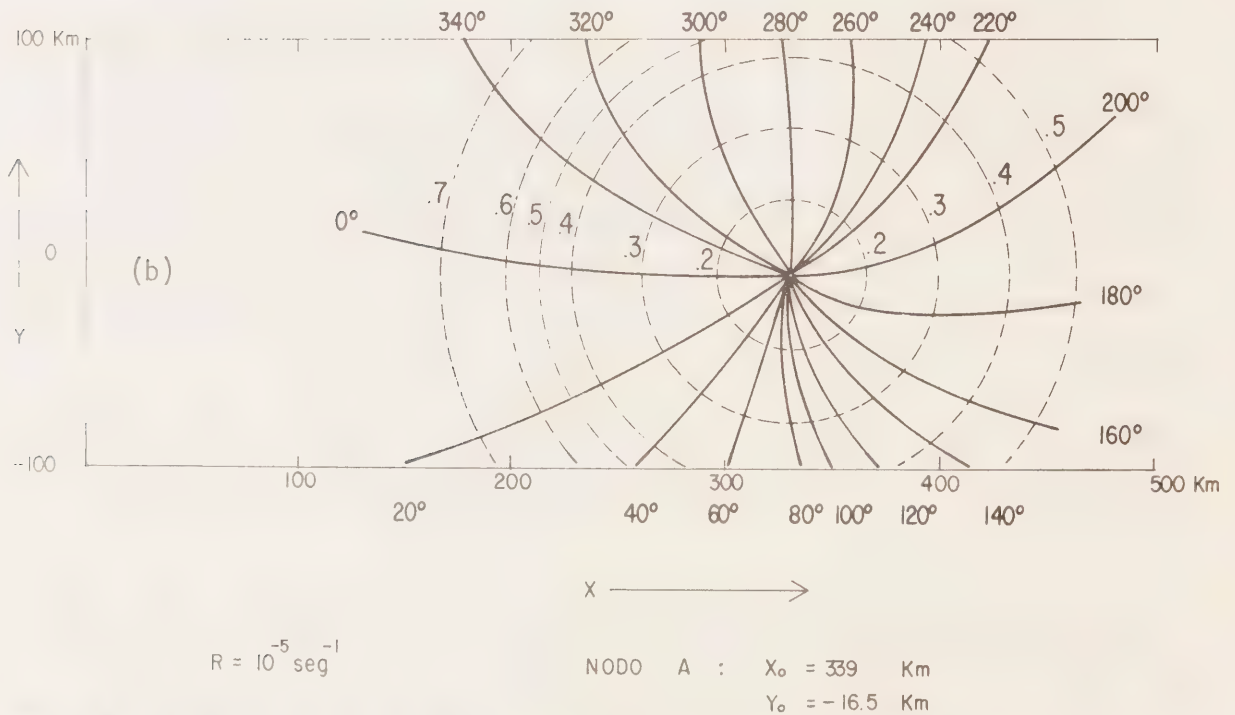
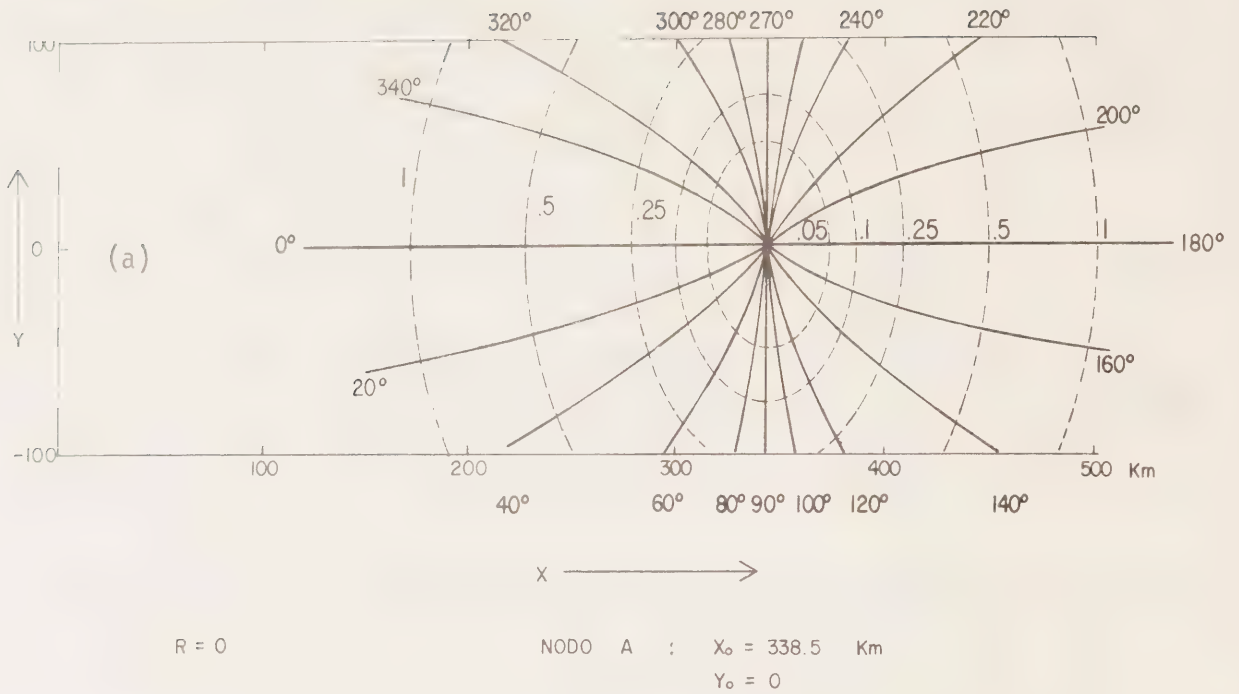


Fig. 5. Cotidal chart of the vertical displacement Z for a standing Kelvin wave corresponding to the frequency of M_2 in a basin at latitude 45°N , width 200 km, depth 100 m, closed at $x = 0$ and of indefinite length. (a) Without friction. (b) With weak linearized friction, $r = 10^{-5}/\text{sec}$. (c) With moderate friction, $r = 5 \times 10^{-5}/\text{sec}$. (d) With strong friction, $r = 10^{-4}/\text{sec}$.

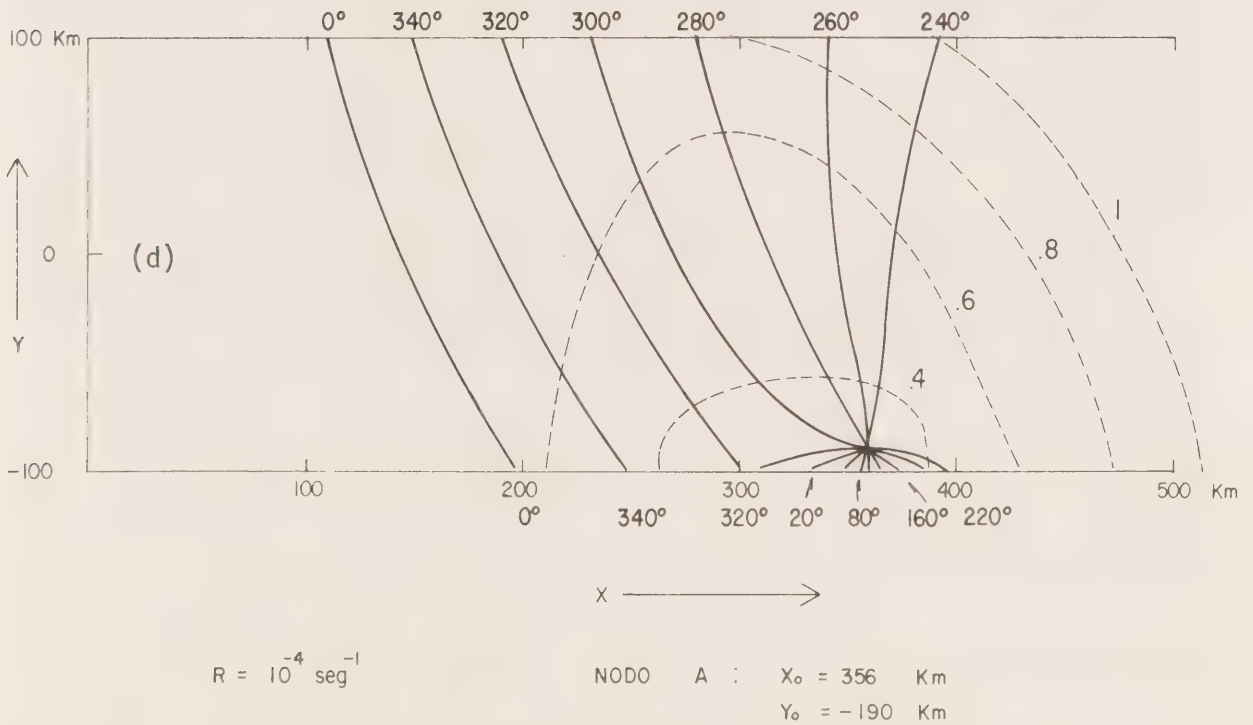
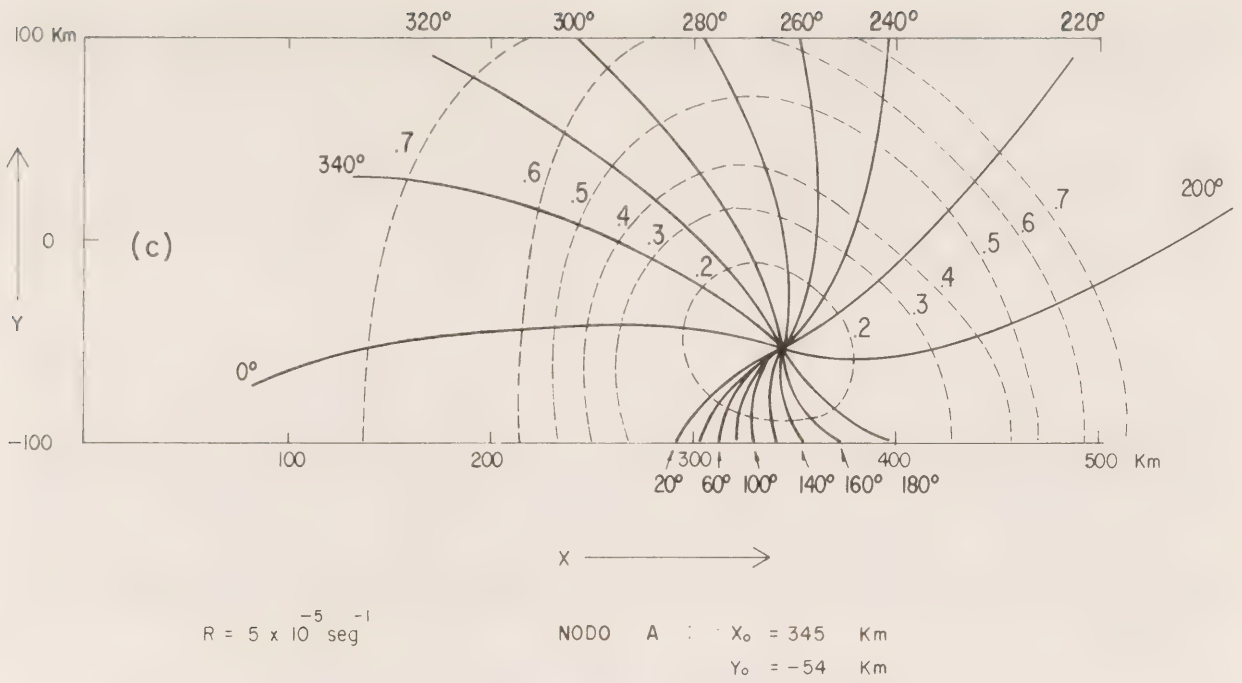


Fig. 5. (Concluded)

The node of the vertical tide Z will be found at the point (x_0, y_0) whose position is such that $\cos(k'x_0 - im'y_0) = 0$ or such that:

$$k'x_0 - im'y_0 = (2n+1)\pi/2 \quad \text{where } n = 0, 1, 2, 3, \dots$$

For $n = 0$, the position of the node is given by:

$$k'x_0 - im'y_0 = \pi/2 \quad (32)$$

and since k' and m' are complex numbers, (32) is equivalent to two linear equations which, when satisfied, give the coordinates of the node. In terms of real numbers:

$k' = a - ib$ $m' = c + id$ where a, b, c and d are real numbers using their definition in (31). Equation (32) is then equivalent to the linear equations:

$$ax_0 + dy_0 = \pi/2 \quad bx_0 + cy_0 = 0$$

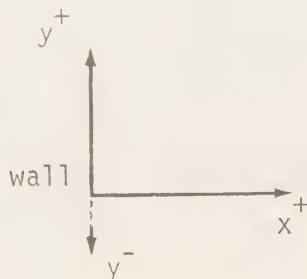
equating real and imaginary parts. Their solution gives the coordinates of the node displaced by friction:

$$x_0 = \frac{\pi}{2} \frac{c}{(ac - bd)} \quad y_0 = -\frac{\pi}{2} \frac{b}{(ac - bd)}$$

Usual values of friction are such that $a > b$ and $c > d$ so that the numerator is positive. Keeping terms to first order with the approximation $a \approx k = \sigma/\sqrt{gH}$ we get $x_0 \approx x'_0 (1 + bd/ac)$, so that the node is pushed away from the reflecting surface by friction. We have written x'_0 for the original coordinate of the node for the case of no friction:

$$x'_0 = \frac{\pi}{2} \frac{\sqrt{gH}}{\sigma}$$

Similarly the negative sign of y_0 indicates that friction pushes the node to the right of the reflecting wall (northern hemisphere):



When the value of y_0 is larger than the half width of the basin, the node falls outside the basin and is said to be "degenerate" or "virtual". This is a common occurrence for either strong friction or very narrow channel.

We will see that with these elementary notions of periodic wave motion, of nodes and of standing Kelvin waves modified by friction, we are able to interpret intelligently the cotidal charts we have drawn for Canada.

5. TIDAL PATTERNS

The tide observed at various harbours has traditionally been described as semidiurnal, mixed or diurnal depending on whether its succession of high and low waters occurs at regular intervals of six hours, at irregular intervals (which can stretch between 3 and 12 hours) or at regular intervals of 12 hours. The type of tide found at a given site depends on the relative amplitude and phase of the harmonics making it up. The semidiurnal constituents overwhelm the diurnal ones in a semidiurnal tide, etc.

If one scrutinizes the tide at many sites it becomes obvious that there is a smooth and gradual transition from one record to the next, so that one is faced with the need to develop a criterion which permits the characterization of the tide at a given site and the development of a system of classification of the various patterns. A criterion much used in the past is the quotient of the sum of the amplitudes of K_1 and O_1 to that of M_2 and S_2 , as it served an immediate measure of the relative importance of the diurnal and semidiurnal signals. The use of such a criterion requires a preliminary harmonic analysis. Advances in computer techniques now permit the objective description of whatever phenomenon that can be described by numbers with the help of so called "patterns" (Batchelor 1972). These can be calculated from records and from these values we may draw charts of patterns similar to cotidal charts and describe visually and quantitatively the various types of tides encountered (Godin 1977). In our restricted use tidal patterns are sets of numbers and labels which help describe, recognize and classify tidal records. They are calculated from second moments of first and second differences of observed tidal elevations spaced 3 or 12 hours apart. These moments take characteristic values for various types of tides and one may put some order into them by referring them to predefined "pure" tides. Once the moments are calculated and compared with those of the pure tides the pattern of any record will fall at some point inside the scale given below:



where S is semidiurnal, N is normal, M is mixed and D is diurnal. The S and M categories are always accompanied by a number smaller than one; the reverse holds for N and D. The pattern numbers move smoothly from S to N and M to D; we call the points of junction, 1.0N and 1.0D. The boundary between M and N is not as sharp; patterns with $\ll 1M$ could very well fall into $\gg 1N$ just

for a very slight change in the value of the second moment of the 12 hour first difference. This however causes little practical difficulty. To indicate this situation we mark by a wavy line the approximate zone of demarcation through which the tide goes from a mixed to a normal character and an arrow indicates the direction where the normal region lies.

Note that the classifications S, N, M and D do not exactly coincide with our intuitive conception of these words. First we recall that tidal patterns merge smoothly one into the other and that there are no sudden jumps in character as the different labels in these categories might suggest. Essentially one could say that the S, N and M patterns describe "semidiurnal" tides as we conceive them intuitively, except that in the S category the diurnal inequality is little marked and that in the M category it becomes increasingly noticeable. These classifications were elaborated from the spectrum of the tidal potential. The N classification contains tides which have diurnal and semidiurnal signals in nearly the same proportion as in the tidal potential; if less (< 1), it is called S (semidiurnal) because this part of the signal is larger than in the applied force. If the diurnal contribution is more than that in the potential, we enter eventually the M and D categories.

Figure 6 shows the predicted tide for April 1978 for a set of stations whose patterns span the scale just indicated. We have chosen stations for which we have good records; as a consequence we could not illustrate all the discrete values of the patterns. An inspection of the figure allows us to follow the evolution from a highly semidiurnal tide to a very mixed tide with prolonged episodes of purely diurnal activity. It must be kept in mind however that the profiles we obtain for April will not be exactly reproduced during other months. Inspection of the profiles indicates that the succession of high and low water becomes appreciably distorted beyond patterns $> .6M$. This marks the practical limit beyond which the computation of the conventional lunitidal intervals becomes questionable. As well this puts us in a position to define precisely what we mean by a "semidiurnal" tide: these are the tides which fall in the categories N, S or whose pattern number is $< .6M$. For all the areas of the chart where this criterion applies we need to use only the M_2 chart to deduce the mean tidal amplitude (and range) as well as the mean time interval between the lunar transit and the occurrence of high or low water. We use Tofino as an example. Its station number is 8615 and its geographical location is $49^{\circ}09'N$ $125^{\circ}55'W$; the pattern number is .161M so that the tide at Tofino is "semidiurnal", just as defined. The M_2 chart gives $A = 99$ cm $g = 241^{\circ}$. As a consequence the mean amplitude of the tide at Tofino should be 99 cm, the mean range 198 cm, the mean lunitidal interval for high and low water should be 8.3 and 14.5 h respectively (the low water for M_2 follows the high water by 6.2 solar hours). Statistical calculations on the observed times and heights of high and low waters at Tofino indicate that the mean range is 213 cm while the mean lunitidal intervals for high and low water are 8.3 and 14.5 h respectively; the M_2 chart supplies a fair approximation to the mean range and the mean lunitidal intervals wherever the tide is "semidiurnal".

The pattern numbers used to elaborate the chart have been derived from the set of analyzed constituents for the given stations; they could have been deduced as well from the hourly observations on the water level. We have chosen the first alternative because it minimizes the effect of the noise.

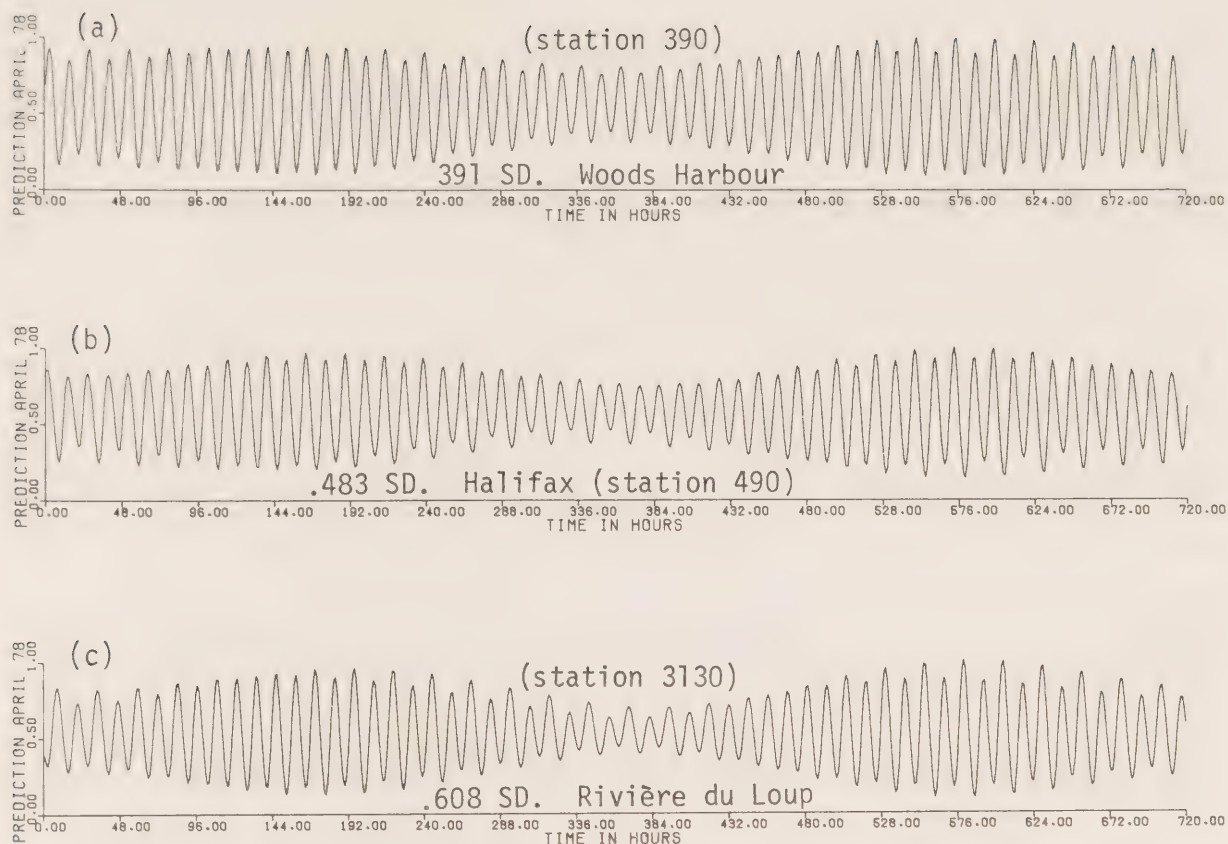
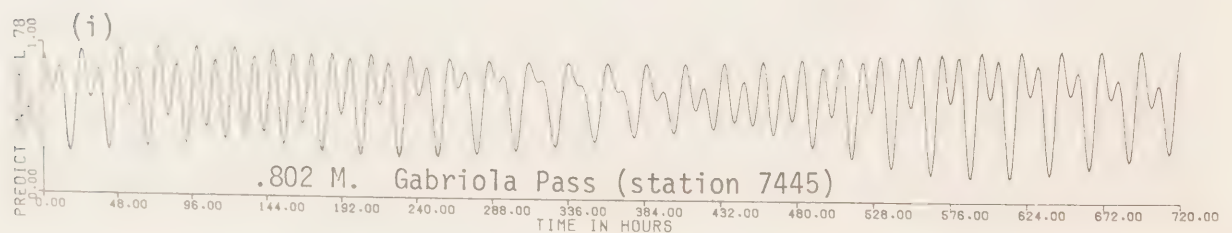
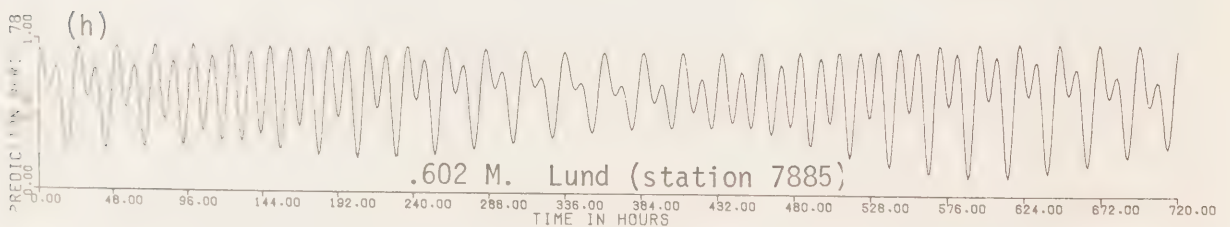
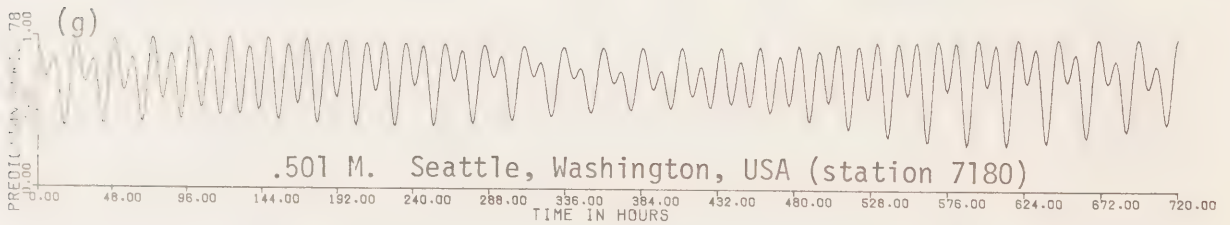
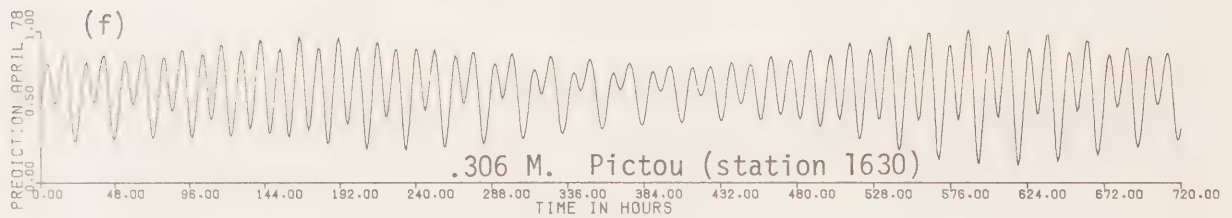
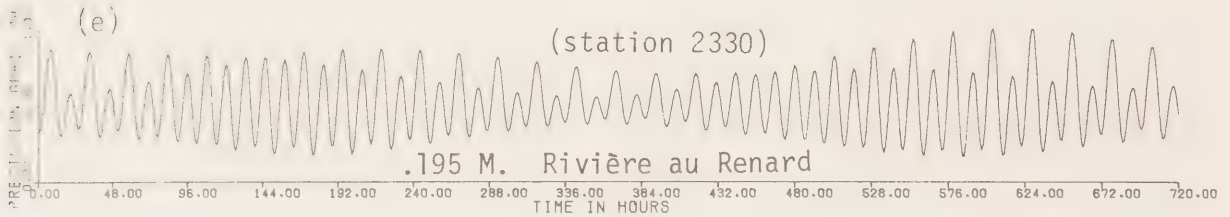
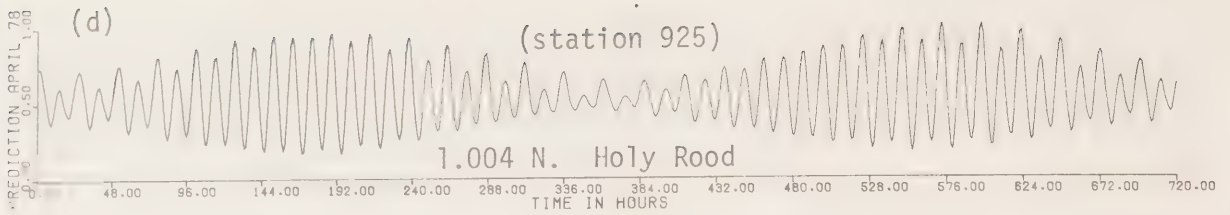
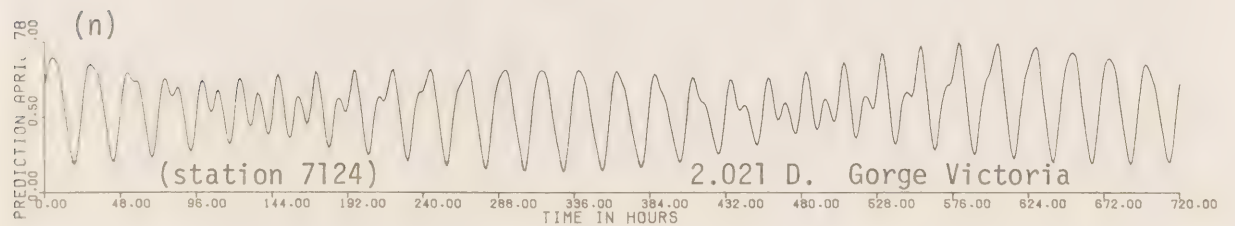
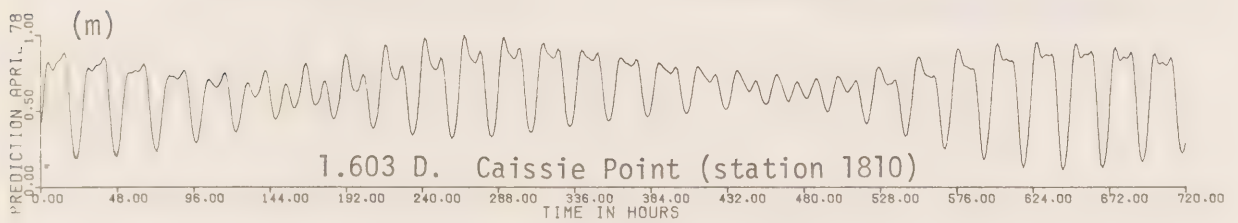
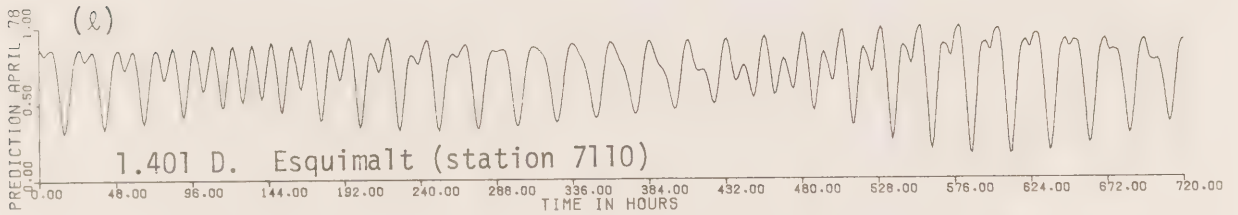
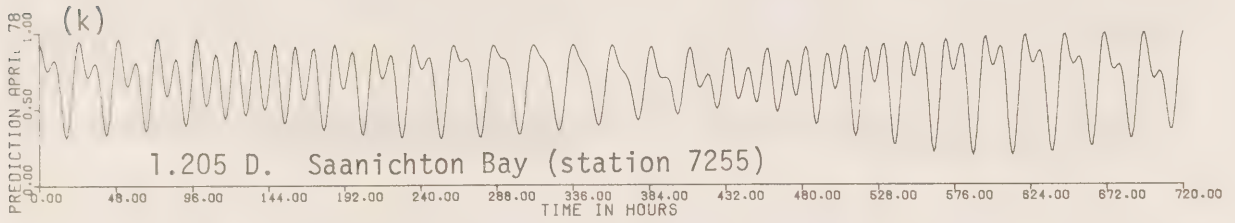
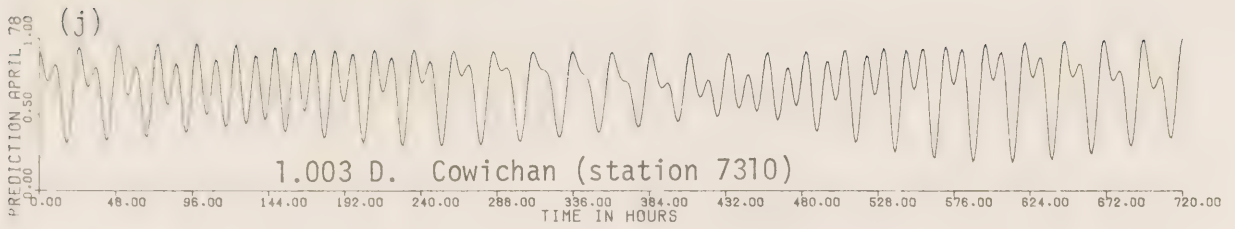


Fig. 6. Set of predicted levels for April 1978 at various stations to illustrate some actual tides corresponding to the indicated patterns. The stations chosen cover patterns from .4SD (almost pure semidiurnal) to 2.0D (almost pure diurnal). (a) 391 SD. Woods Harbour. Good semidiurnal tide with a slight diurnal inequality. (b) .483 SD. Halifax. Quite similar to Woods Harbour with a more marked diurnal inequality and more intense change from springs to neaps. (c) .608 SD. Rivière du Loup. Still a good semidiurnal tide with an even more marked change from springs to neaps. (d) 1.004 N. Holy Rood. We enter the normal category where the spectrum of the constituents is very similar to that of the tidal potential. (e) .195M. Rivière au Renard. We enter the M (mixed) category where the diurnal portion of the spectrum of the constituents becomes larger than that in the tidal potential. The diurnal inequality is quite marked during the two semimensual maxima in the lunar declination which occur around hour 288 and hour 624 of the month. (f) .306 M. Pictou. (g) .501 M. Seattle, Washington, USA. (h) .602 M. Lund. (i) .802 M. Gabriola Pass. (j) 1.003 D. Cowichan. We enter the D (diurnal) category where the probability increases that there will occur a single tide over a span of 24 hours. (k) 1.205 D. Saanichton Bay. (l) 1.401 D. Esquimalt. (m) 1.603 D. Caissie Point. This station lies to the southwest of the semidiurnal point of amphidromy which exists in Northumberland Strait. (n) 2.021 D. Gorge Victoria. Apparently the record with the most diurnal character available in our files. Both the diurnal and semidiurnal bands of the mixed tide entering from Victoria are damped while it propagates into the Gorge but the semidiurnal band is damped more rapidly.





Shallow water tides have patterns which fall in the range just described, but the fact that their low water is clipped at about the same height for all tides necessitates the calculation of an additional index which is defined by:

$$m_2(d_3)/.252 \equiv I$$

where $m_2(d_3)$ is the second moment of the second differences between hourly observations spaced 3 hours apart. The value of I for any shallow water stations will be > 1 while for other stations it is < 1 (and not calculated).

6. COMMENTS ON THE COTIDAL CHARTS

We have drawn the charts for the constituents M_2 , S_2 , N_2 , K_1 and O_1 in order of frequency, as well as charts of the tidal patterns. Technically we should have also drawn the charts of P_1 and K_2 which are also constituents of importance. The reason for not doing so is that these two constituents are not separable from K_1 and S_2 from short records, so that they must be inferred. Once their values are laid out on a chart, a good proportion of them cannot be treated as true data but only as a direct inference from the constituents mentioned. Since on the other hand their value must be included in the preparation of predictions, we may use the ratios and phase differences given (Fig. 7) to calculate them from the amplitude and phase of K_1 and S_2 . The figure gives the vectors r and ϕ , where r is the amplitude ratio and ϕ the phase difference, of P_1 to K_1 or K_2 to S_2 actually found in the course of one year analyses at stations where there was sufficient data to separate them. The vector average of all the r and ϕ for a given region, as seen from the diagram, is sufficient to give an adequate estimate of these additional constituents.

The constituents actually illustrated fall into two species, diurnal and semidiurnal. M_2 predominates in the semidiurnal band and K_1 in the diurnal, while the maps of N_2 , S_2 and O_1 tend to be quite similar to those of M_2 and K_1 . As a consequence our comments will be limited in general to the maps of M_2 and K_1 , although the maps of O_1 , N_2 and S_2 are also necessary to make predictions at a given point of the ocean.

In areas of the maps where the patterns fall to the left of $.6M$, one may use the map of M_2 exclusively to estimate the mean time of travel of the tide from one point to another and the mean range at a given point. For example, if we look at the location of Port aux Basques and St. John's we note that the local values of M_2 are 44 cm 14° and 35 cm 315° . Twice the amplitude gives 88 cm and 70 cm and the phase difference is equivalent to 2 h 2 min in time. The observed mean range at Port aux Basques and St. John's is 94 and 77 cm respectively; the mean time difference between high or low water between the two stations is 1 h 57 min.

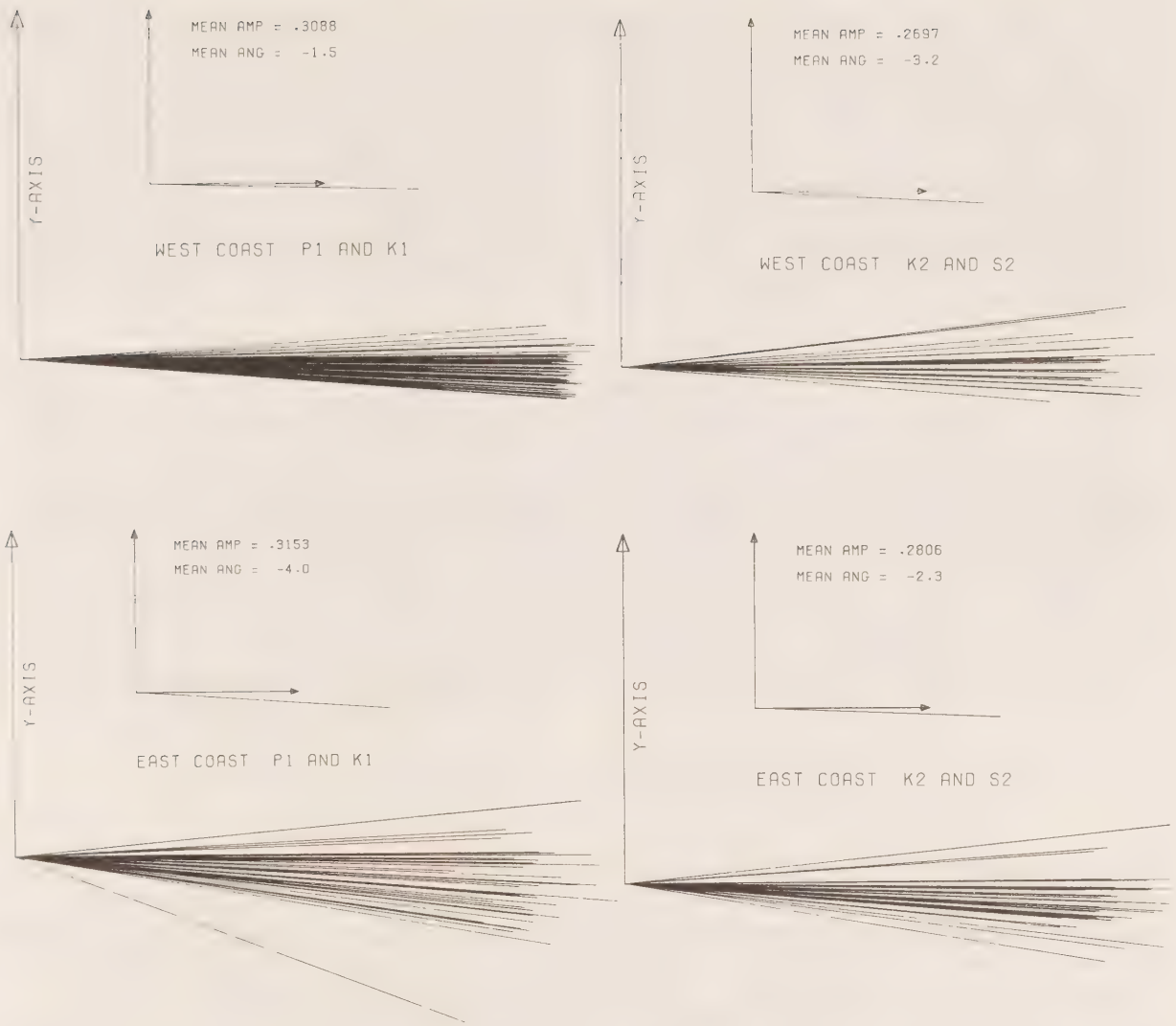


Fig. 7. Observed amplitude ratio and difference in the Greenwich phase lag between the pairs K_2 and S_2 , P_1 and K_1 . It is presented as a vector of length r (amplitude ratio) and inclined at an angle ϕ (difference of phase lag). These values are obtained at stations where the constituents are separable; they are used afterwards for inferring K_2 from S_2 and P_1 from K_1 at stations where they cannot be separated. Since the observed values depend on the geographical location, the measured vectors are presented in groups for the west coast and east coast. The tendency of the vector to bunch around the common value indicates that a mean value exists for the vector and the vector mean is presented in each case. The actually observed r , ϕ values are shown as rays in the larger diagram. Their vector average is shown in the smaller diagram as a single ray whose amplitude (\bar{r}) and orientation ($\bar{\phi}$, in degrees) are written out explicitly as "mean amplitude" and "mean angle".

6.1 Charts for Canada

The charts (Fig. 8) show the tidal régime in all ocean waters adjacent to Canada and illustrate the effective response of these waters to the tide in the neighbouring Atlantic, Pacific and Arctic Oceans and to the local semidiurnal and diurnal tidal forces. In each the solid contours denote co-phase lines along which the vertical displacement associated with the specific constituent is simultaneous. The phases are measured in degrees and correspond to the Greenwich phase lag in the Greenwich time zone ($Z = 0$). The tidal wave progresses in the direction of increasing phase. The time interval Δt corresponding to a given phase difference $\Delta\phi$ may be obtained with the help of the following rule:

$$\Delta t = \frac{\Delta\phi}{\sigma} \text{ hours} \quad (33)$$

where σ is the frequency of the constituent given previously. For example, a phase difference of 20° between two contours is equivalent to:

$$\Delta t = \frac{20}{28.98} \text{ h} = 41 \text{ min for } M_2$$

$$\frac{20}{15.04} \text{ h} = 80 \text{ min or } 1 \text{ h } 20 \text{ min for } K_1$$

Grossly one may say that 1° of phase is 2 min of time in the semidiurnal band and 4 min of time in the diurnal. The dashed contours are lines of equal amplitude and the units are centimeters. The contour interval is not regular and varies with the density of observations, the speed of change and the space available to draw them. Therefore while studying the maps one must always watch for a sudden change in gradient, either in phase or in amplitude. It did not seem reasonable to draw regular and smooth contours in areas where there is virtually no information. On the other hand we had no fear of extrapolating contours in areas of more but still little information or of conjuring amphidromic structures wherever the sparse data suggest one.

We recall that the charts are of the vertical tide only; this represents an incomplete picture of the tidal movement as it ignores the horizontal displacement or tidal current. In theory we can draw charts of Z or u with equal ease, whereas in practice the prospect as to when we will be able to draw charts of the tidal currents as actually observed is still remote.

6.1.1 Nodes and antinodes

We recall that the wavelength of K_1 is approximately twice

Fig. 8. Cotidal charts for the constituents M_2 , S_2 , N_2 , K_1 and O_1 in waters adjacent to Canada. A Miller projection is used for the geographic background. The solid lines are contours of constant Greenwich phase lag; the dashed lines are contours of constant amplitude and the units degrees and centimeters. The contours are marked as 120° or 30 to indicate a Greenwich phase lag of 120° or a contour of 30 cm. The time zone used for all the maps is Greenwich ($Z = 0$). The spacing of the contours is not necessarily regular. Question marks indicate areas where it was not possible to conjecture the type of motion present either because of a shortage of data or of their poor quality. The signs + or - help visualize the direction of increasing or decreasing values in areas where this is not evident. (a) M_2 (b) S_2 (c) N_2 (d) K_1 (e) O_1 .

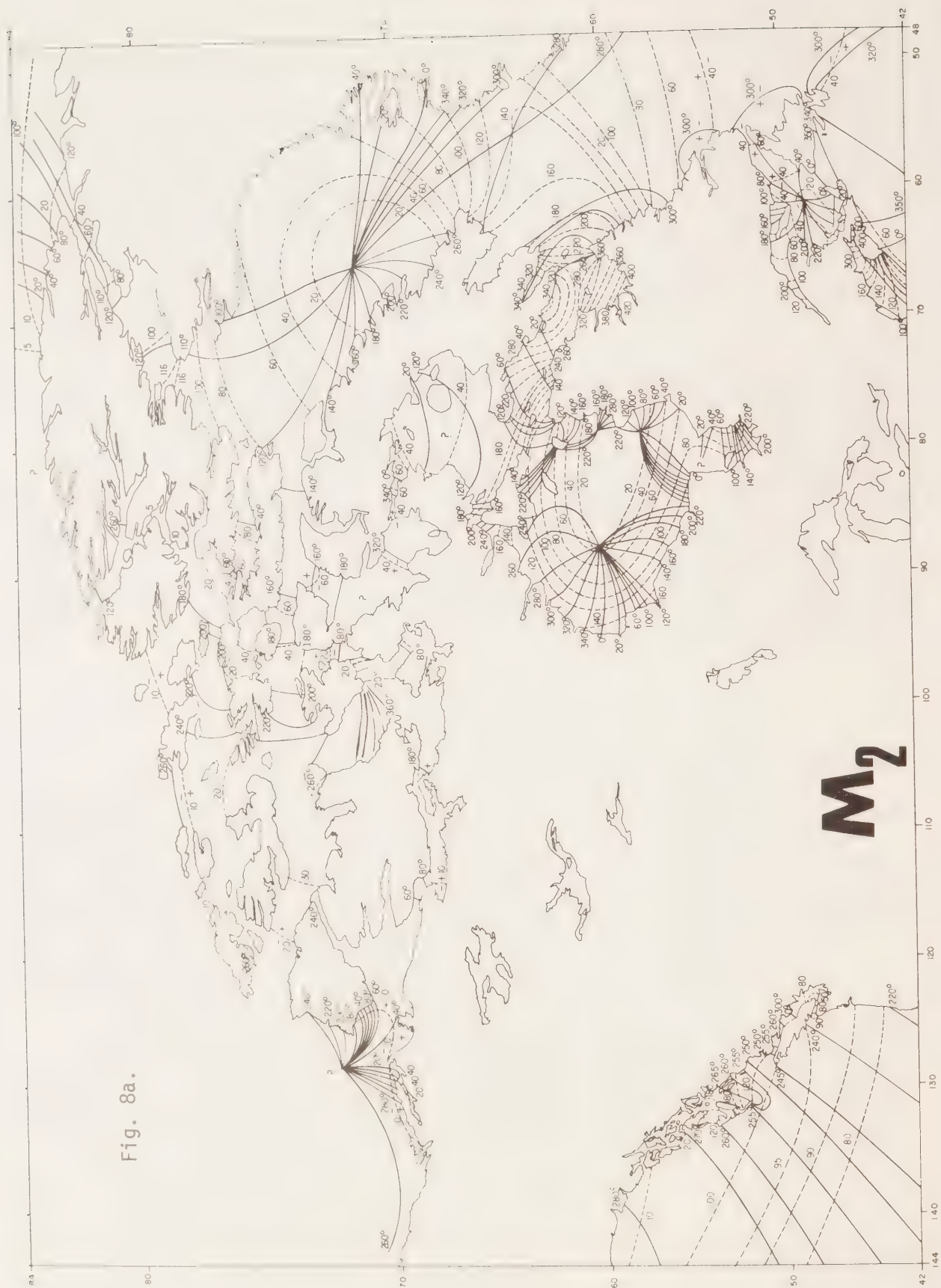


Fig. 8b.



S2

Fig. 8c.



Fig. 8d.

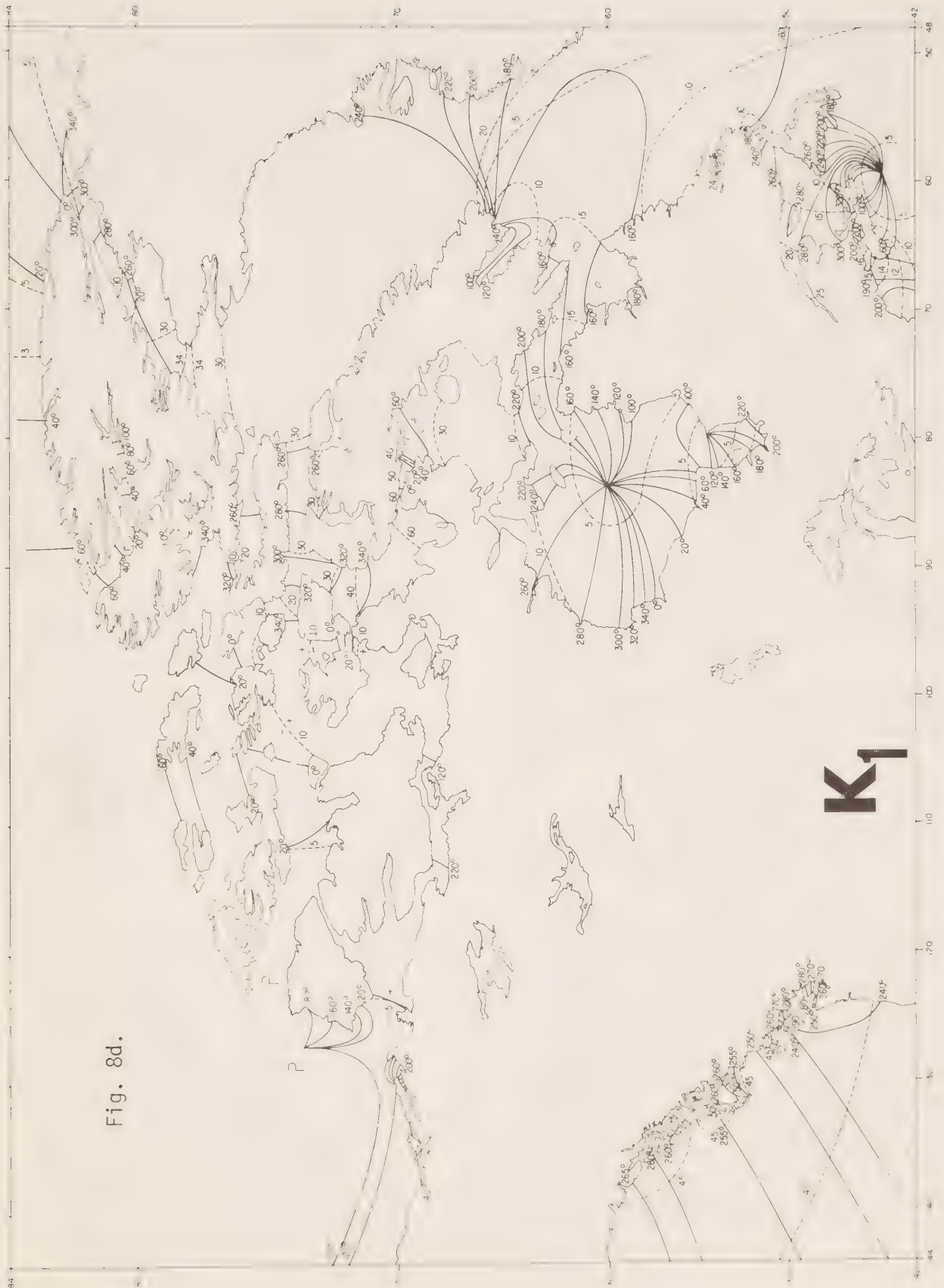


Fig. 80.



that of M_2 in a sea of constant depth, so that an amphidromy in M_2 (Fig. 8a) should imply an amphidromy in K_1 (Fig. 8d) further away from the reflecting wall. We find a well-defined amphidromy of M_2 in Baffin Bay, off Clyde Inlet. The corresponding node of K_1 falls on the Cumberland Peninsula and is degenerate. We note that friction displaces both nodes to the right of the reflecting wall, which in this case is the coast of Greenland at latitude 76°N in Nares Strait. The second amphidromic system for M_2 is found in the Gulf of St. Lawrence and the corresponding node of K_1 falls outside the gulf, south of Cape Breton Island and west of Sable Island. We find a second mininode of M_2 in the northern portion of Northumberland Strait.

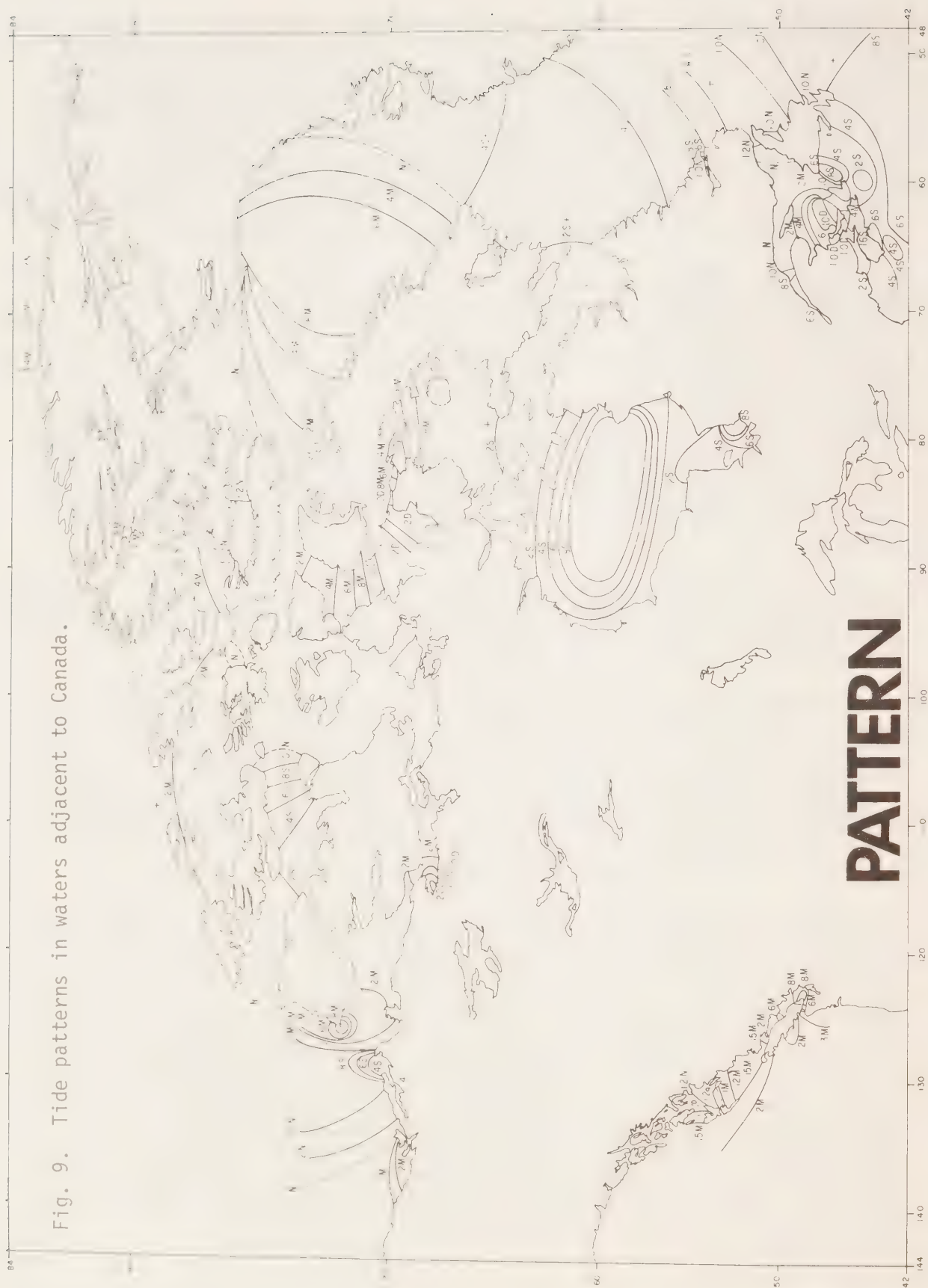
There is evidence of amphidromic systems in Hudson Bay; they appear quite complicated because of the shape and shallowness of the bay. There are probably four semidiurnal nodes in a north-south direction; one lies at the latitude of Mansel Island, probably quite mangled because of the local topography, one to the east of the Ottawa Islands, one south of Inoucouac and finally one inside James Bay at the latitude of Moar Bay. Friction has pushed them well to the right of the reflecting wall (the southern portion of Hudson Bay and James Bay) and the node in James Bay is completely degenerate. Because of the width of Hudson Bay an additional transverse node exists east of Churchill. The diurnal counterpart of the system described consists of a node south of Coats Island and another (degenerate) at Cape Jones.

It is almost certain that an amphidromy exists in the area off Coppermine with another likely in Foxe Basin where shallow depths imply short wavelengths. There probably exists an amphidromy west of Sachs Harbour. We see no evidence of nodes in the North Pacific off British Columbia.

Antinodes are never as obvious as nodes in cotidal charts, nevertheless between two nodes there should always be an antinode. A spectacular example is found in Hudson Strait where it is marked by extreme amplitudes in the semidiurnal band because of resonance and a near absence of cophase lines indicating simultaneous tides over a large area. The corresponding diurnal antinode is found in the Labrador Sea. A more emphatic diurnal antinode is to be found in Committee Bay west of Fury and Hecla Strait where the diurnal tides are as large as those on the west coast in Georgia Strait.

Because of the numerous openings of Canadian basins to the ocean, we encounter areas where the partial waves from various directions come together, areas where "tide meets tide". With the help of cotidal charts we may be quite precise when we speak of "tide meets tide". It is the area where the phase of two waves coming from different directions is the same; in a zone little affected by friction it would also mark the point where the amplitude is maximum. We note for example that tide meets tide to the north east of Queen Charlotte Islands for the case of M_2 , but that the maximum amplitude is further south (Fig. 9). The actually observed tide is made up of the superposition of all the harmonic components and the zone of "tide meets tide" in the observed situation may move from day to day and from neap to spring tide. The phenomenon can be observed in many areas including: Kane Basin in Nares Strait for the semidiurnal tide (the diurnal tide progresses from the Atlantic northward to the Arctic Ocean), the Strait of Belle Isle for both tides and in Hecate Strait.

Fig. 9. Tide patterns in waters adjacent to Canada.



The largest but least obvious example of the phenomenon is found west of the arctic archipelago; the archipelago acts as a complicated conduit through which the Atlantic tide makes its way westward to meet the tide in the Arctic Ocean. The opposite occurs inside the shallow Coronation Gulf which is penetrated by the arctic tide as far as King William Island. We shall see more examples when we scrutinize the larger scale maps.

6.1.2 Areas in need of further exploration

We have indicated in the map of M_2 (Fig. 8a) those regions which are essentially devoid of tidal observations; naturally they fall in the arctic, an immense and quite inaccessible area which will be known only with the help of a systematic and rational program of exploration. A list of the regions which need to be explored are: the Canadian shore of the Arctic Ocean from Banks Island to Greenland; inside the arctic archipelago; Amundsen Gulf; Coronation Gulf, McClintock Channel and the Gulf of Boothia; Foxe Basin and the northern entrances to Hudson Bay; the west coast of James Bay from Cape Henrietta Maria to Sand Head; the east coast of Ungava Bay; the Bay of Fundy and the east coast of Hudson Bay. I mention this region last because it presents some special difficulties. Study of the records of Inoucjouac indicates that the locally weak and fickle tides are very much affected by the formation of an ice cover; the range varies by 60% and the mean time of arrival of the tide may vary by one hour from season to season. Therefore some special care must be taken before developing a plan for measurements there.

6.2 Patterns of tides

We can draw contours of the amplitude and phase of the constituents σ , as well as of patterns of tide (Fig. 9). Such a map shows at a glance the various types of tide present and where they are to be found. The nodes delineate zones of rapid changes in patterns because of the steep gradients in amplitude they imply; therefore we shall meet pure D or pure S tides at the sites of the nodes we noted previously. We see such areas in the shallows around the Magdalen Islands, in Northumberland Strait, south of Cape Breton Island, in Hudson Bay and in Baffin Bay.

The tide is strongly semidiurnal south of the Maritimes and Newfoundland, in Hudson Strait and in the Bay of Fundy. It is mainly semidiurnal in the Labrador Sea, in the northern section of the Gulf of St. Lawrence and in the arctic archipelago. It is strongly diurnal in Committee Bay. It has a weakly mixed character along the Pacific west coast, which indicates the existence of an appreciable diurnal inequality. It acquires a more mixed character in Juan de Fuca and Georgia Straits because of a degenerate semidiurnal node around Victoria.

In all areas of the map where the character of the pattern is left of .6M, we may compute lunital intervals and ranges unambiguously.

7. LARGE SCALE MAPS

7.1 British Columbia

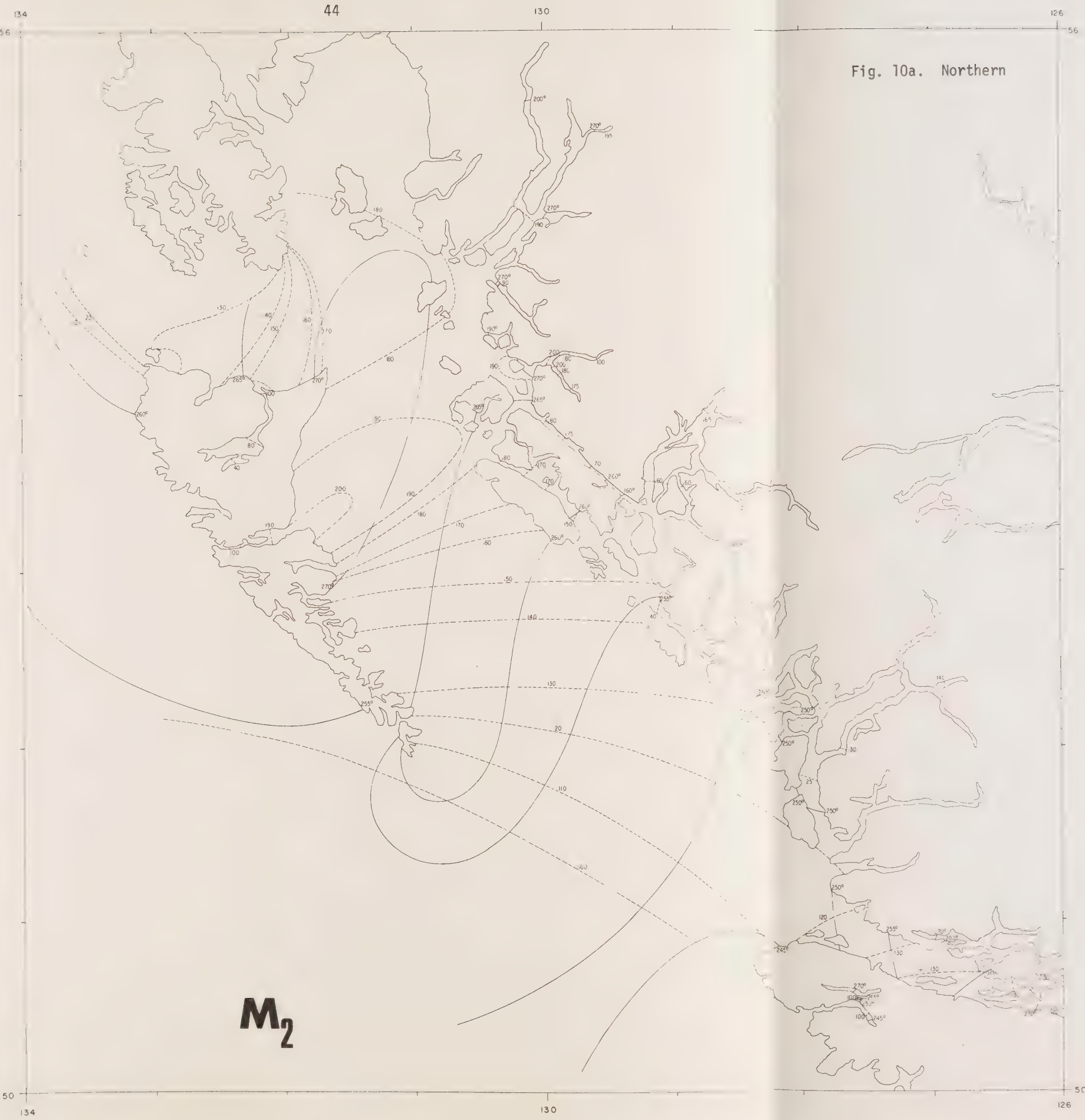
The small scale maps (Fig. 8) indicated that the tidal motion in our section of the Pacific is relatively simple and consists of a counterclockwise progression of the crest of high water with increased amplitude northward. The large scale (Fig. 10) shows additional details east of the Queen Charlotte Islands and east of Vancouver Island. The map for each constituent is given in two sheets; one covering the northern section from Alaska to Vancouver Island, the other the southern section around Vancouver Island. The tidal motion gets more complicated than in the open Pacific and consists essentially of the breaking up of the tidal wave into northern and southern branches. A finer scale motion consists of the progress of the tide up the numerous fjords indenting the coast in which the details of the motion are of local interest only.

In the north the semidiurnal Pacific wave enters Hecate Strait from Dixon Entrance and from the broader Queen Charlotte Sound. There is a zone of simultaneous phase between Rose Point and Skidegate Inlet with a more defined zone of maximum amplitude off Skidegate Inlet. This holds as well for S_2 and N_2 . This area defines a zone of "tide meets tide" where large tides are usually accompanied by weak currents. The progress of the tide inside the various inlets is indicated wherever information is available.

In the south the local geography creates further complication in the progress and development of the tide. Once again the Pacific semidiurnal wave divides into two branches, the northern one entering through Queen Charlotte Strait and the southern one through Juan de Fuca. Because of the shallowness of Juan de Fuca a semidiurnal node is formed at the longitude of Victoria-Esquamalt which is degenerate. There is a delay of $2\frac{1}{2}$ hours between the entrance of the tide in Juan de Fuca and its passage by Victoria. The degenerate amphidromy retards it further and then also the Gulf Islands, so it emerges into Georgia Strait five hours after its entrance into Juan de Fuca. There is some complicated motion inside the Gulf Island caused by the local geography, which has been described elsewhere (Godin 1976) but in Georgia Strait itself the tide is effectively quasi-simultaneous as far as Campbell River. Here we see a good example of a zone of antinode, the constricted geography in the north acting as an effective barrier to the semidiurnal wave entering through Juan de Fuca. The northern branch of the semidiurnal wave progresses normally as far as Johnstone Strait. Further south it is effectively blocked by the system of narrows north of Georgia Strait. We note extreme delays of the order of two hours within a span of 10 nautical miles in Seymour Narrows and Hoskyn Channel. It enters Georgia Strait with a phase equal to that of the wave coming from the south indicating the limit of progress of the northern wave.

The M_2 wave in the Pacific has an amplitude of 90 cm in the southern sections of British Columbia increasing to 110 cm near Alaska. The M_2 signal is further amplified in Hecate Strait and reaches a maximum of 200 cm off Skidegate. In the south the reverse occurs in Juan de Fuca where the M_2

Fig. 10. Cotidal charts for the constituents M_2 , S_2 , N_2 , K_1 and O_1 in waters adjacent to the northern and southern portions of British Columbia. (a) M_2 (b) S_2 (c) N_2 (d) K_1 (e) O_1 .



M₂

Fig. 10a. Northern

Fig. 10a. Southern

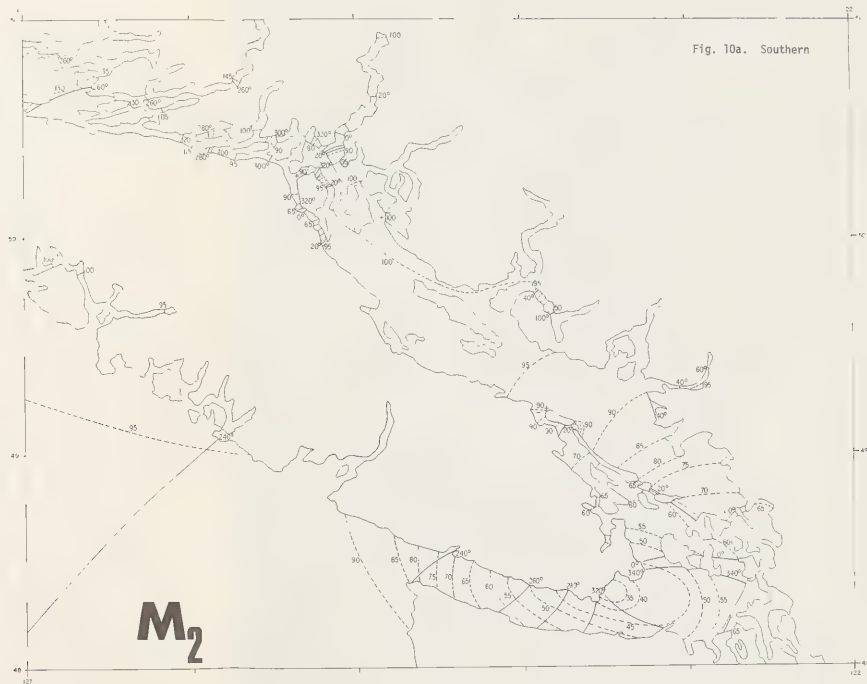


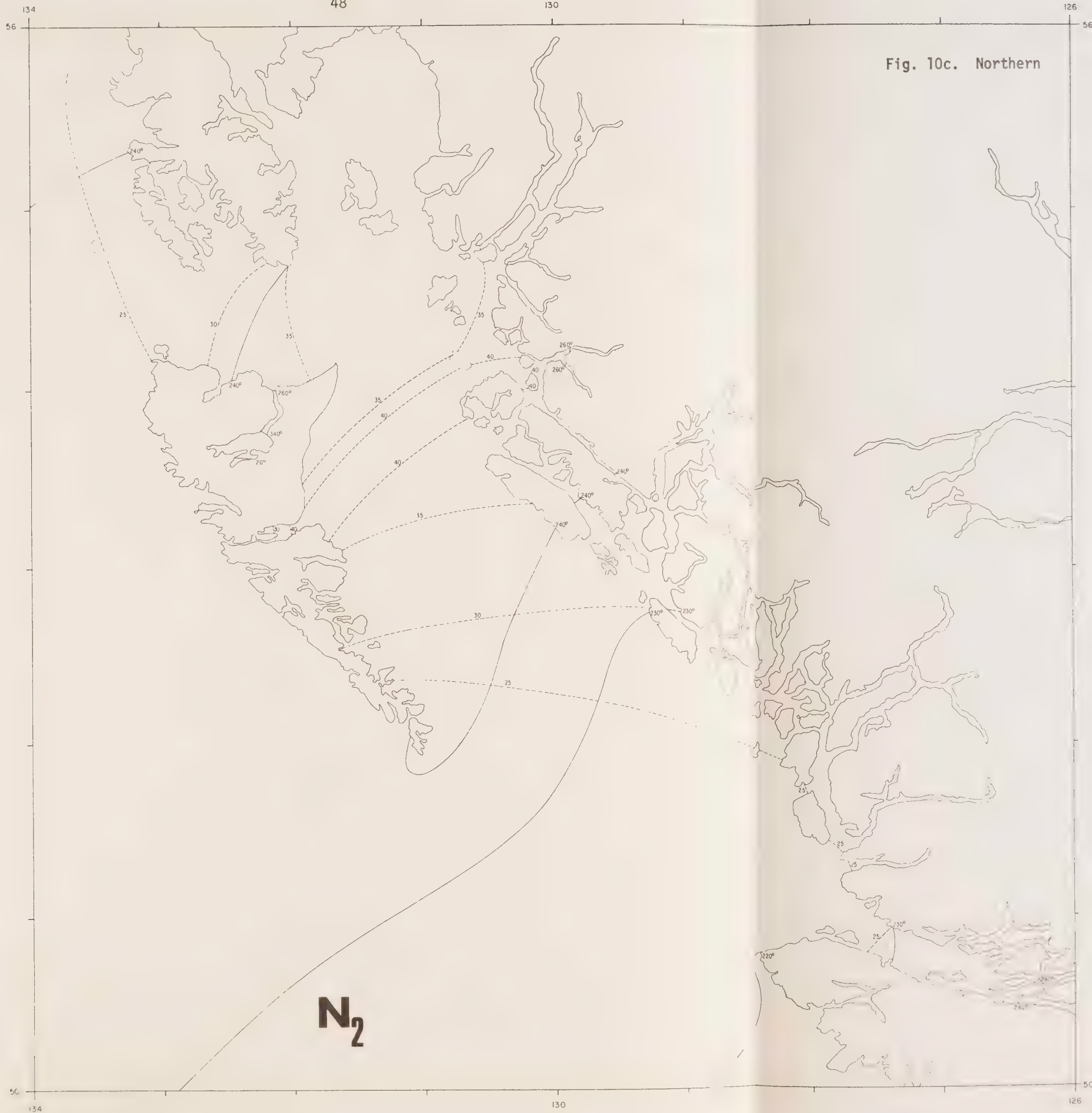
Fig. 10b. Northern

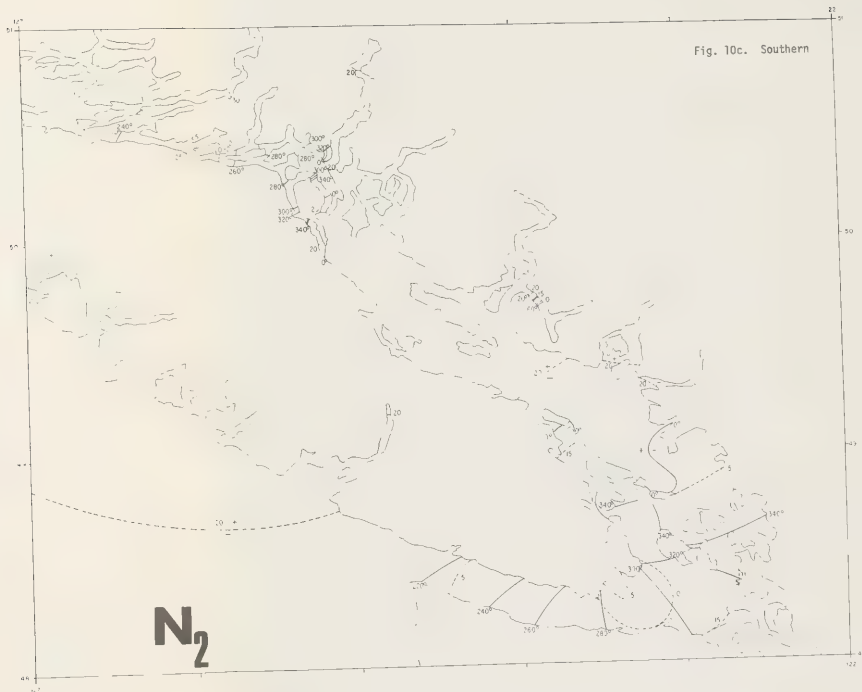
Fig. 10b. Southern





Fig. 10c. Northern







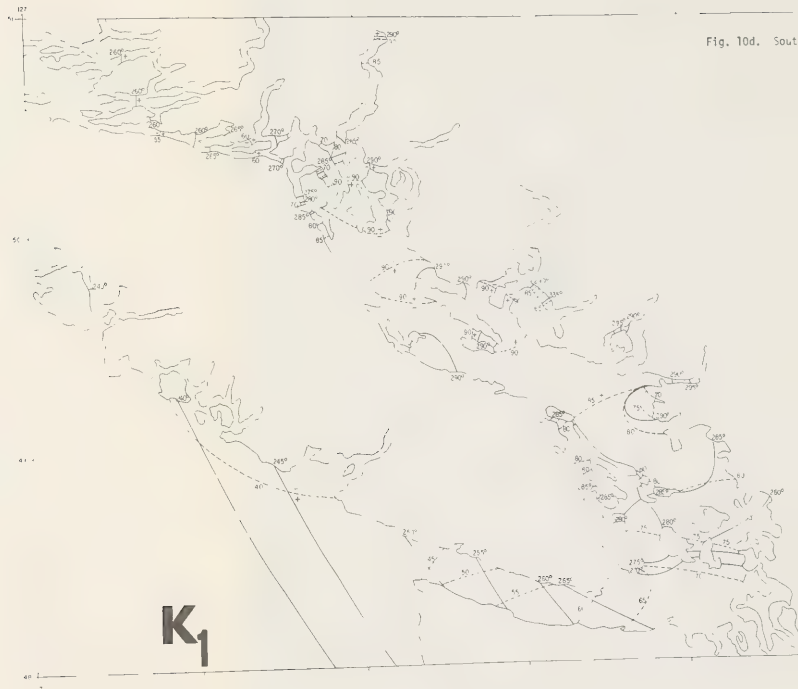
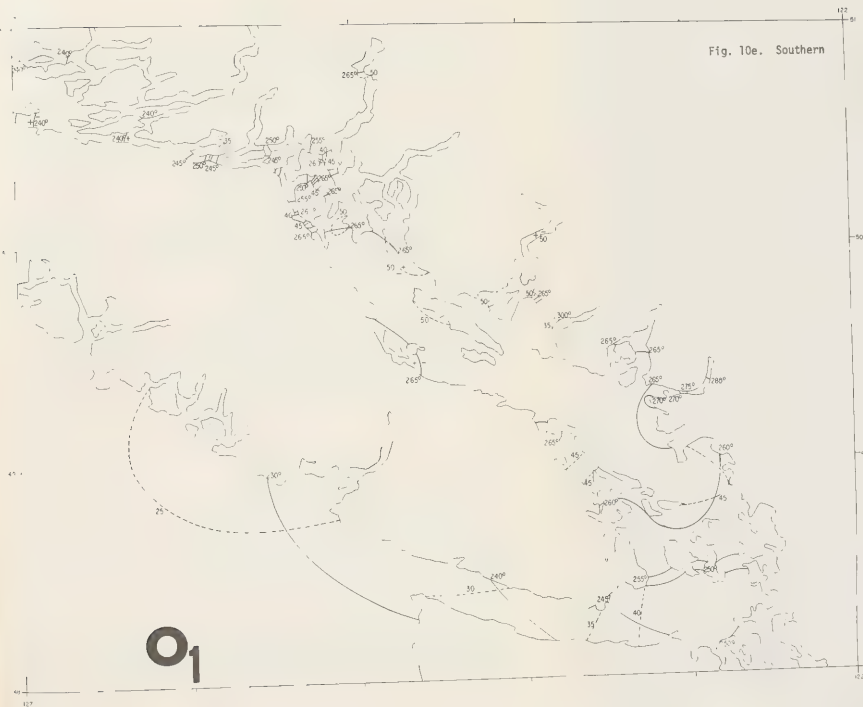


Fig. 10e. Northern



Fig. 10e. Southern



amplitude decreases from 90 cm at the mouth to 35 cm off Victoria-Esquamalt. The degenerate amphidromy creates an east-west gradient in amplitude towards Admiralty Inlet. Thereafter the amplitude increases rapidly through the Gulf Islands and the transverse gradient disappears eventually in Georgia Strait. In the northern entrance the M_2 amplitude increases regularly from 100 to 130 cm in the entrance of Johnstone Strait. Losses diminish it after and it gets to 95 cm in the northern entrance to Georgia Strait. A similar description applies equally to the other semidiurnal waves S_2 and N_2 (Fig. 10b and c).

The modification of the diurnal Pacific tide by the Queen Charlotte Islands and Vancouver Island is quite similar to that for the semidiurnal tide; a difference is that the diurnal node equivalent to the node near Victoria-Esquamalt lies outside Juan de Fuca. The K_1 amplitude has a zone of amplitude larger than 50 cm in the northern portion of Hecate Strait. Over the Pacific all along the Canadian coast it has an amplitude of the order of 40 cm. It increases to 50 cm in Queen Charlotte Strait. In Juan de Fuca it increases steadily from 45 cm to 80 cm in its entrance to Georgia Strait. There is no local minimum off Victoria-Esquamalt because of the absence of a diurnal node. Amplitudes larger than 90 cm are found around Texada Island. There is indication that the southern branch of the diurnal wave diffuses somewhat through the narrows north of Georgia Strait.

The patterns (Fig. 11) indicate that the tide in the Pacific has a slightly mixed character. It becomes more normal in Hecate Strait and although the number of contours is quite large, the tide over the whole area has a rather uniform character. This changes abruptly in Juan de Fuca because of the semidiurnal node there and it has a character higher than .6M (mixed) from Port Renfrew all the way to Georgia Strait and beyond Seymour Narrows. The calculations of conventional lunital intervals in that region cannot be too successful because of the presence of intervals during which the tide is diurnal.

7.2 Gulf of St. Lawrence, Cape Breton and Newfoundland

The semidiurnal tide (Fig. 12a, b, c) is dominated by the amphidromy west of the Magdalen Islands. The node is strongly distorted by the presence of the islands and the very few data available seem to indicate that east of the islands there is still a marked semidiurnal signal, thus inducing abrupt gradients in the amplitude contours. We find a second node at the northern end of Northumberland Strait. It may be the same node encountered in the Magdalen Islands which has been split by Prince Edward Island or it may have been created by the local bathymetry. It is still intact for M_2 and N_2 in spite of the narrowness and shallowness of the channel but appears to have been pushed against the coast in the case of S_2 (Fig. 12b).

The movement of the M_2 tide in the Gulf of St. Lawrence, because of the presence of the Magdalen node, consists of the counterclockwise motion of the crest of high water which enters Cabot Strait then progresses along the west coast of Newfoundland, the Québec northshore, Gaspé Peninsula and the northeastern coast of Prince Edward Island. The motion inside Northumberland Strait consists of a wave entering from the south progressing up the strait

Fig. 11. Patterns of the tide in waters adjacent to the northern and southern portions of British Columbia. (a) Northern portion (b) Southern portion.

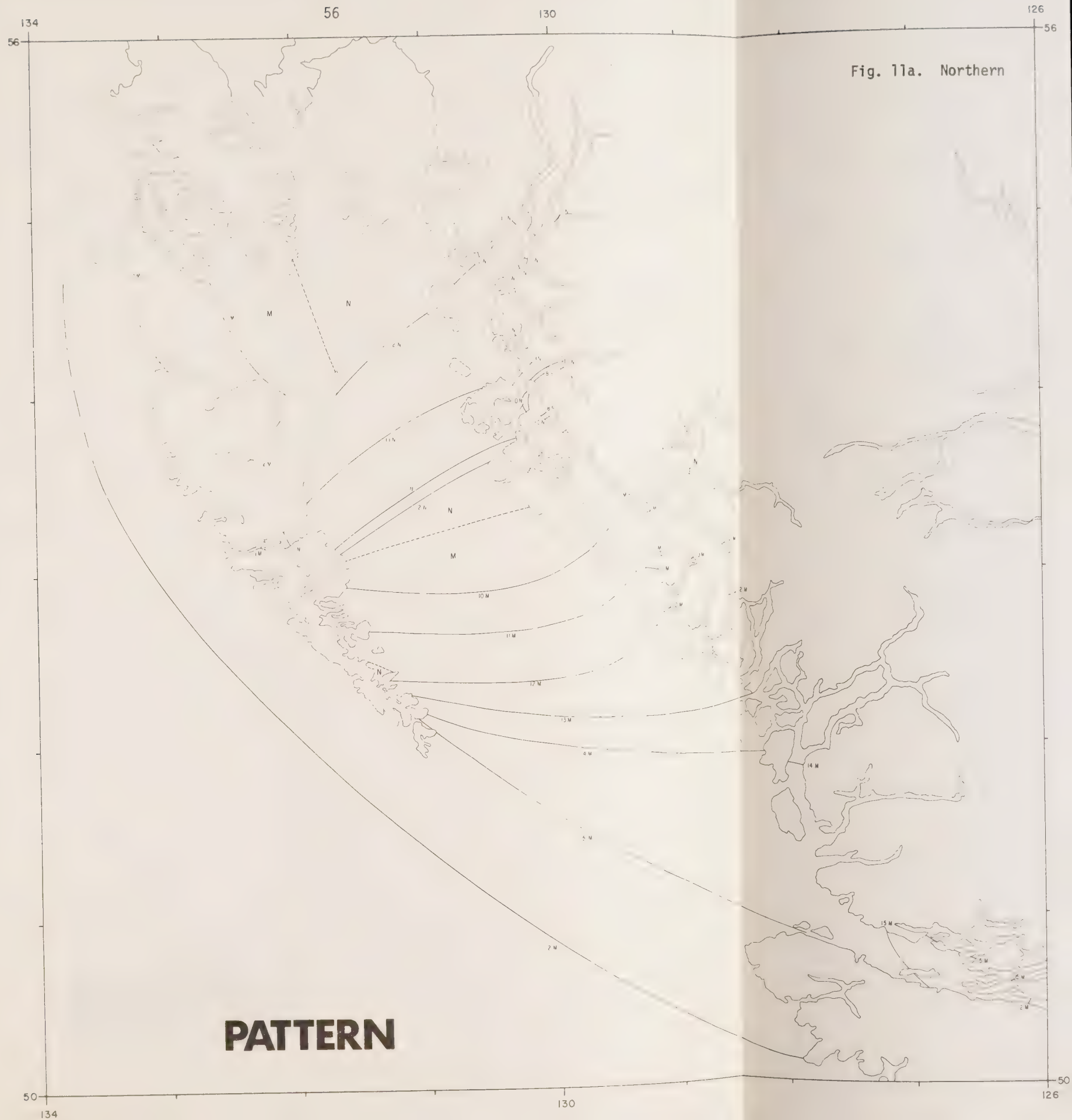


Fig. 11b. Southern

A detailed bathymetric map of the Southern region, likely a coastal area. The map shows various depth contours labeled with values such as 2M, 3M, 4M, 5M, 6M, 7M, 8M, 9M, 100, 110, 120, 130, and 140. The coastline is irregular with many inlets and peninsulas. A large, curved contour labeled '2M' is prominent on the left side. The word 'PATTERN' is printed in large, bold, black capital letters at the bottom left of the map area.

PATTERN

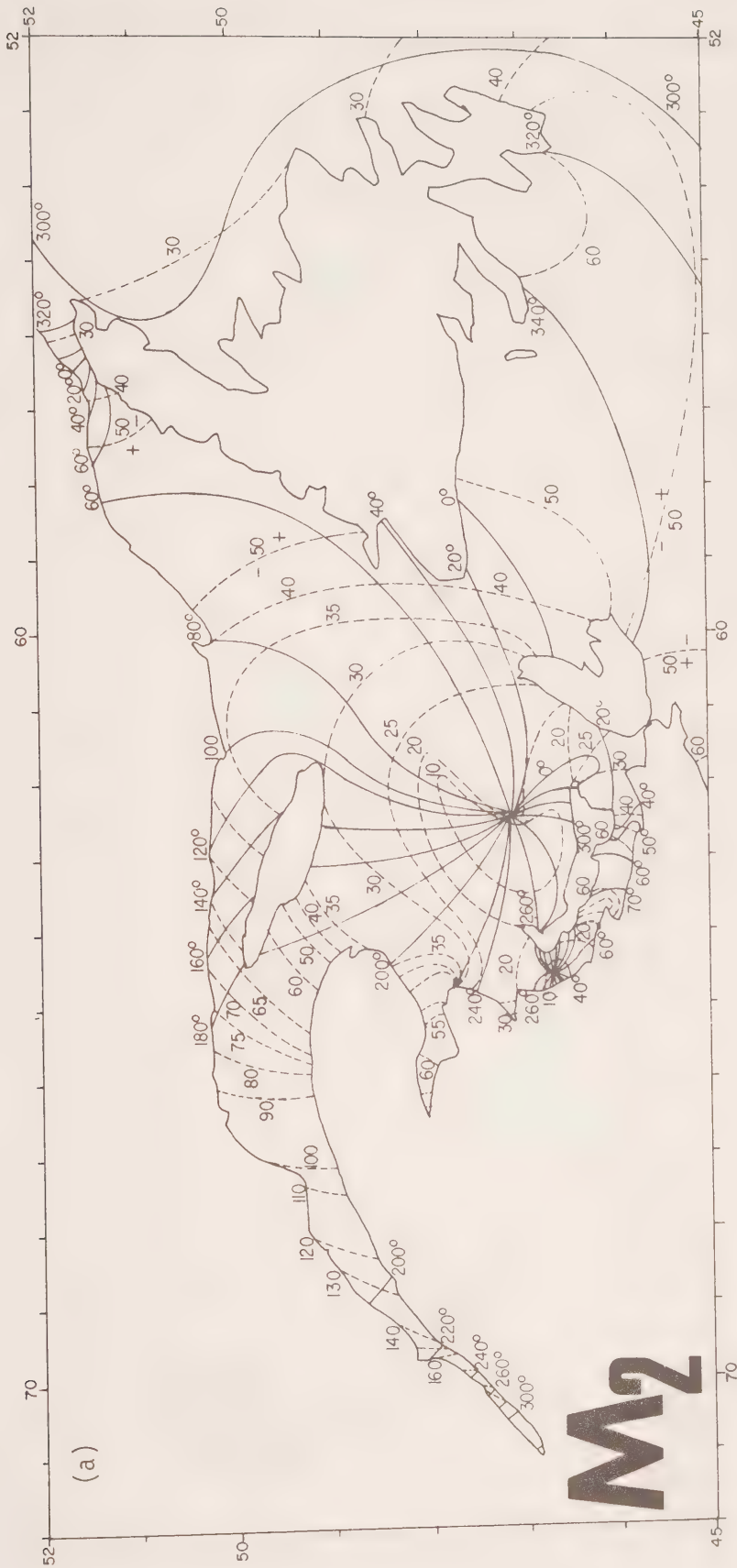


Fig. 12. Cotidal charts for the constituent M_2 , S_2 , N_2 , K_1 and O_1 around Newfoundland and off Cape Breton to the estuary of the St. Lawrence River. (a) M_2 (b) S_2 (c) N_2 (d) K_1 (e) O_1 .

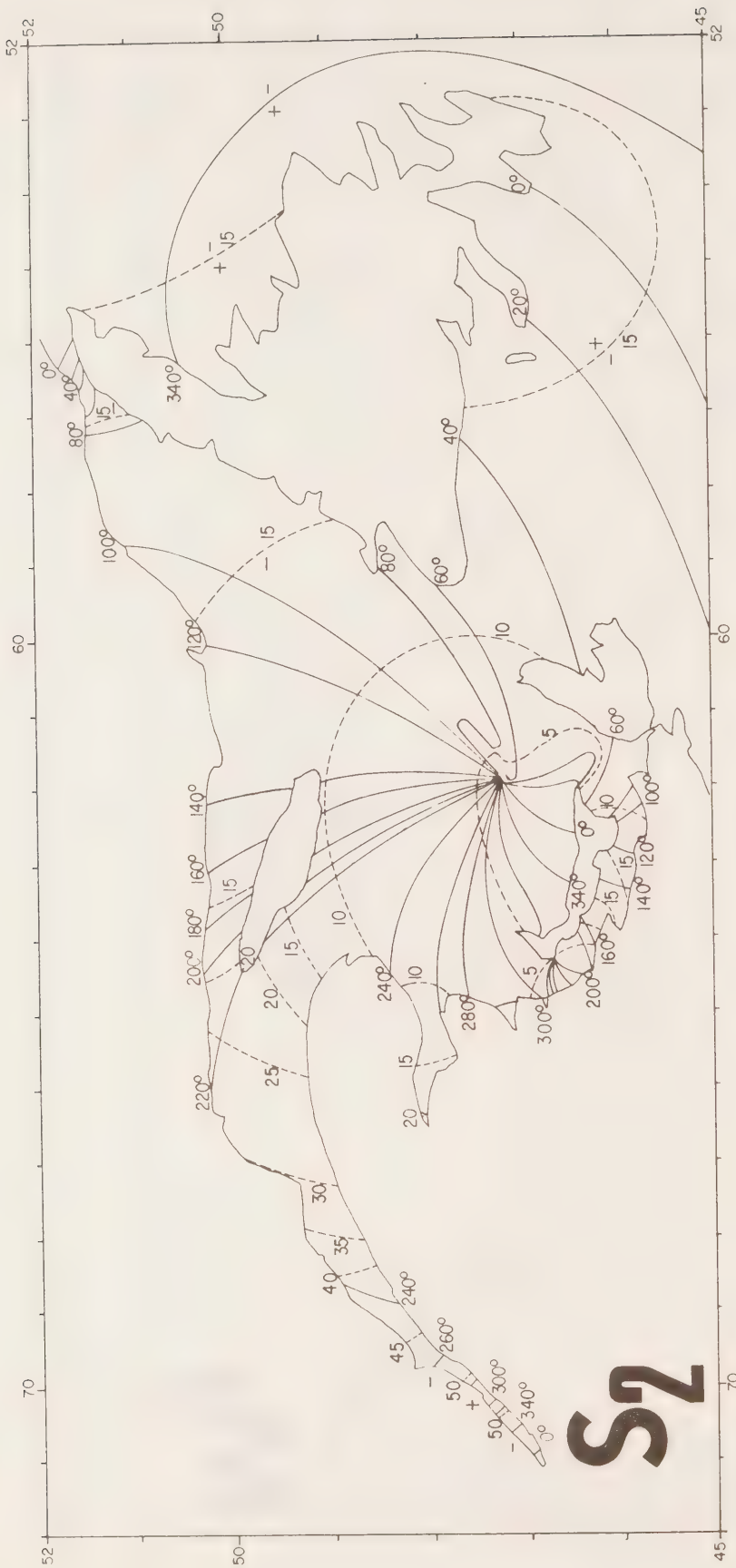


Fig. 12b.

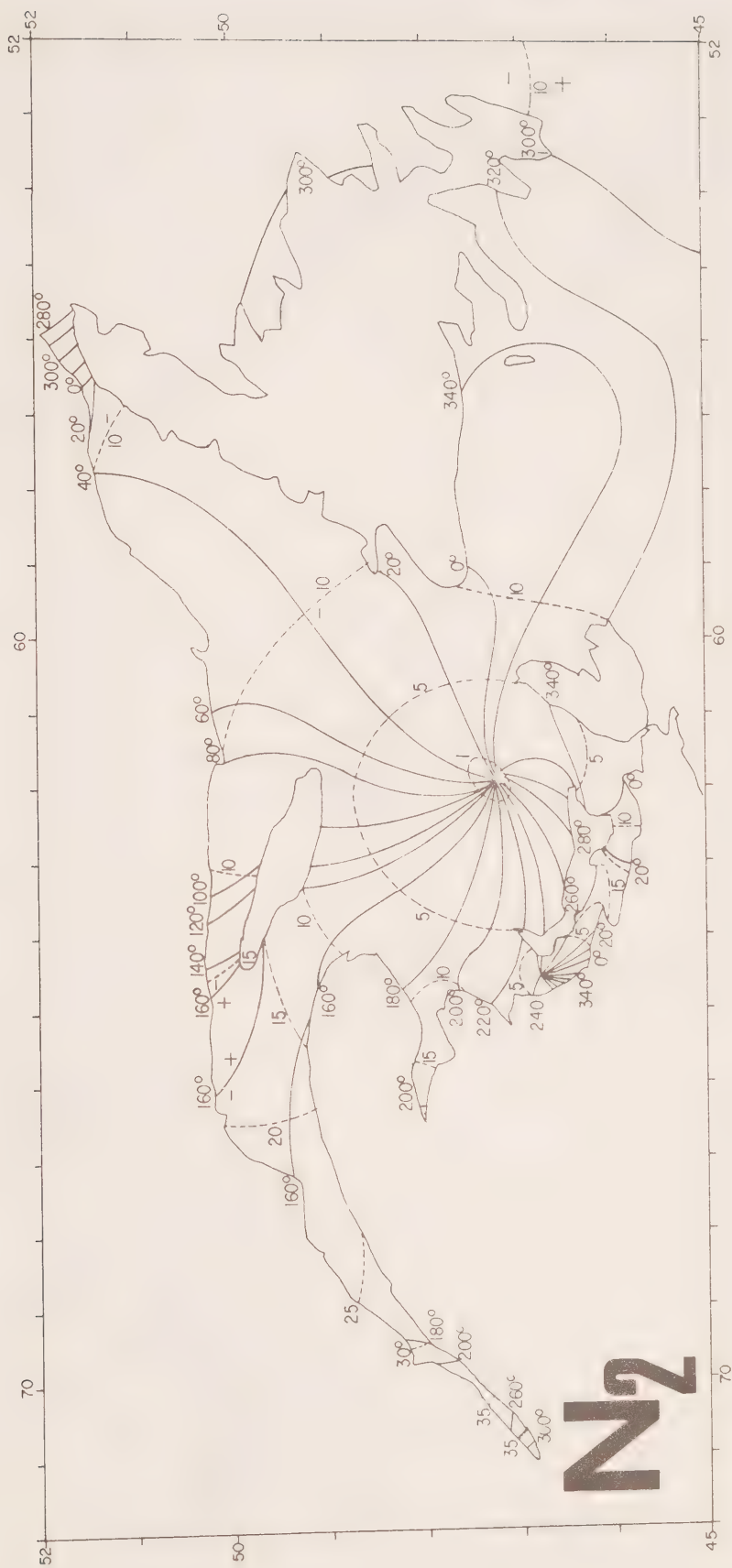
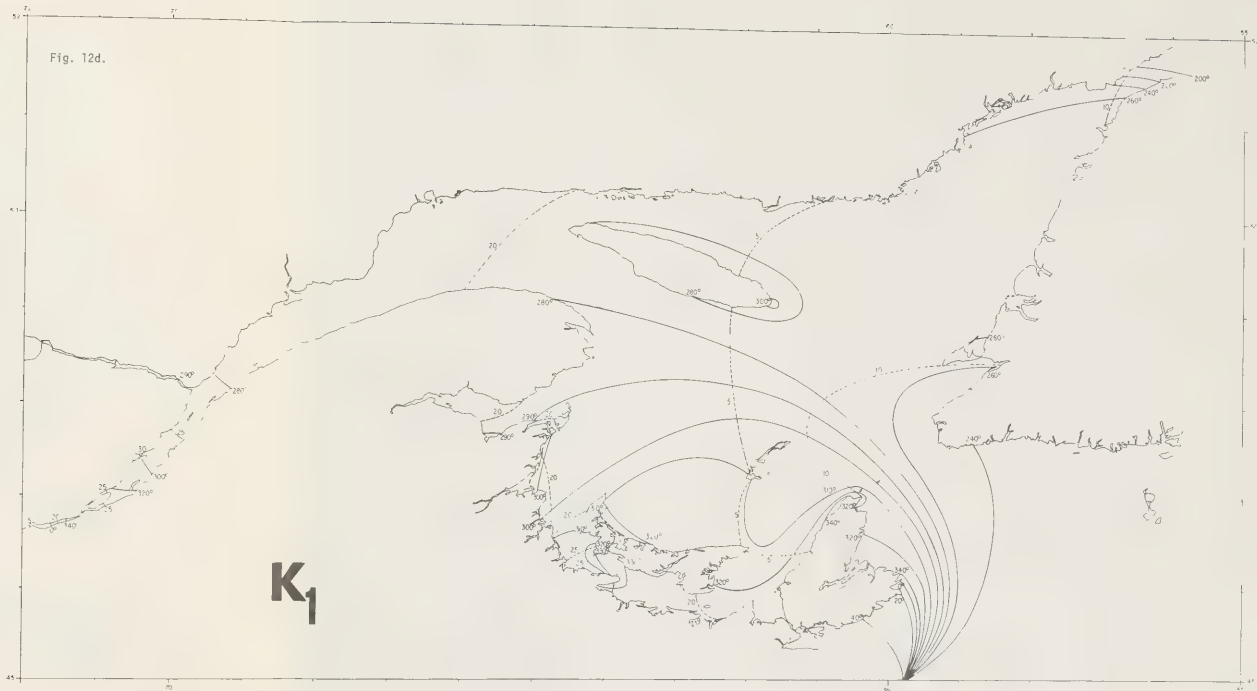


Fig. 12c.

Fig. 12d.



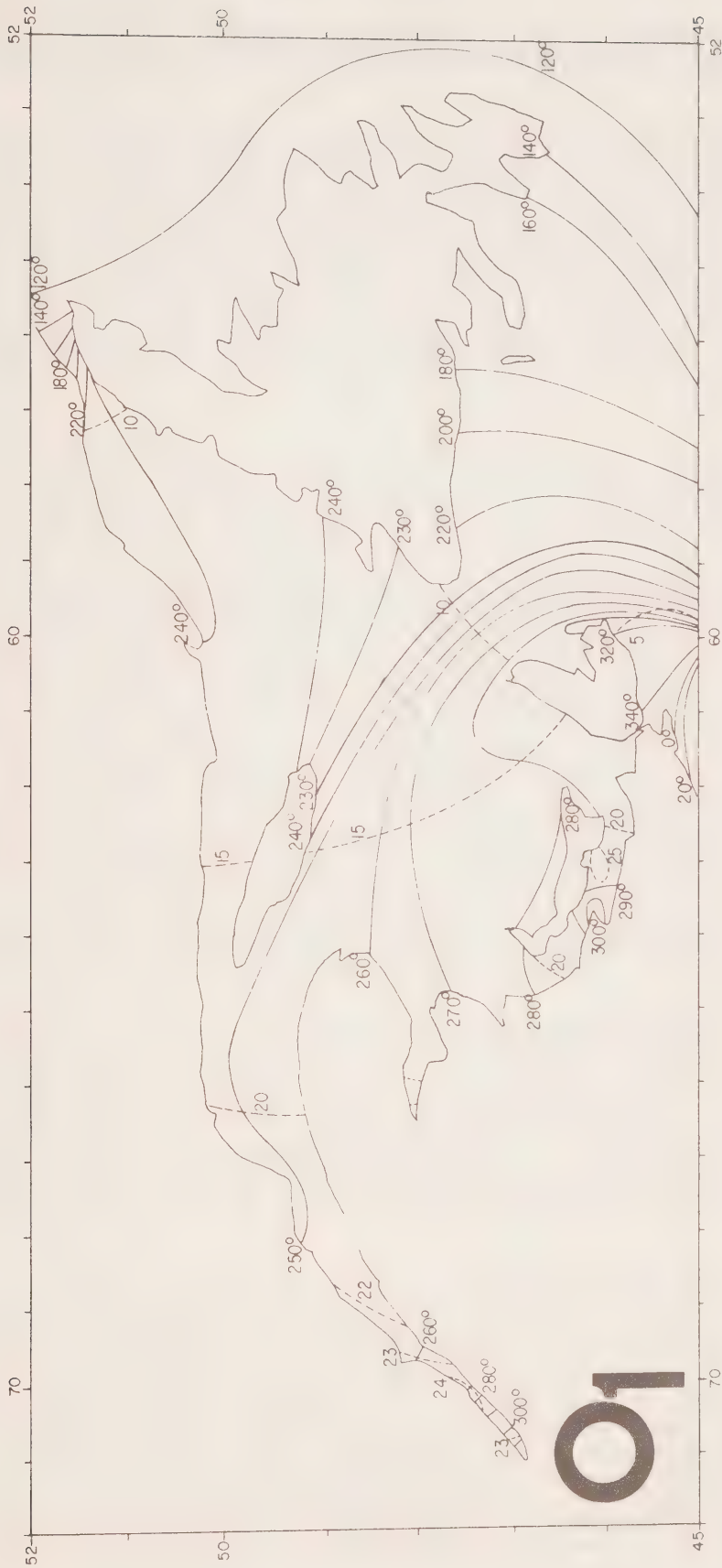


Fig. 12e.

with increasing amplitude until it meets the region of the node, where there is a rapid decrease in amplitude and marked delays in the progress of the tide.

The semidiurnal tide is nearly simultaneous along the east coast of Newfoundland while along its southern shore, it starts progressing towards Cabot Strait taking about two hours to reach it. Past the Gaspé Peninsula it takes a progressive character and travels towards Québec with continuous amplification. The maximum amplitude is found between Isle aux Coudres and the eastern tip of Ile d'Orléans. There the channel splits and the depth decreases, friction takes over and the tide acquires an increasing shallow-water character. It takes eleven hours to progress from Québec to Sorel at the western extremity of Lake St. Peter beyond which it is no longer detectable.

The K₁ tide (Fig. 12d) inside the Gulf of St. Lawrence presents a simpler picture, because its node lies outside and it treats the Gulf area as far as Pointe des Monts and the Strait of Belle Isle as an integral part of the Atlantic Ocean. There is a time delay of over 5 hours between the diurnal peak at Port aux Basques and North Sydney. It meets the Belle Isle branch of the wave well inside the gulf, just north of Anticosti, because the Strait of Belle Isle is also quite permeable to the diurnal signal. On the other side it progresses towards the Magdalen shallows and splits in two branches north and south of Northumberland Strait. The diurnal tide is virtually simultaneous along the east coast of Newfoundland (Fig. 12e) and like the semidiurnal tide it starts progressing along its southern shore towards Cabot Strait taking nearly 7 hours. Because it has a small amplitude in the open Atlantic and in the gulf area, the diurnal tide is of secondary importance. It is amplified in Northumberland Strait and off the New Brunswick coast, creating local diurnal inequalities. The diurnal tide takes a progressive character in the St. Lawrence estuary increasing in amplitude as far as the Ile d'Orléans. Thereafter it is increasingly delayed and distorted by friction; it is no longer detectable past Louiseville in the middle of Lake St. Pierre having taken 11 hours to reach it from Québec (Fig. 13).

Semimonthly tides are perceptible at Montréal (Fig. 14) although there are no regular tides as we know them near the seashore. This tide is created mainly by the nonlinear interaction of M₂ and S₂ and reflects the occurrence of spring and neap tides downstream by rises and falls in the local level. The effect becomes apparent at Cap à la Roche and reaches a maximum at Trois-Rivières where it exceeds in amplitude the regular tide. It is quite faint but still perceptible in Montréal where effects of the river discharge are also apparent.

The patterns in the geographical area which we investigate are quite complicated because of the nodes (Fig. 15) except along the east coast of Newfoundland where they are almost uniformly of the N category. South of Newfoundland they move rapidly from the .4S (strong semidiurnal) category to the N (normal) category in Cabot Strait. The patterns in the northeastern section of the gulf hover around the boundary of the N and M category. From Anticosti to the Magdalens they shift rapidly from .2M (slight diurnal inequality) to 2.0D (diurnal). They are mixed along the north shore of Prince Edward Island and they pass through the M and D category inside Northumberland Strait. In the estuary the tide reverts to slightly mixed then to the

Fig. 13. Cotidal charts for the constituent M_2 , S_2 , N_2 , K_1 and O_1 in the upper St. Lawrence River. (a) M_2 (b) S_2 (c) N_2 (d) K_1 (e) O_1 .

Fig. 13a.



Fig. 13b.



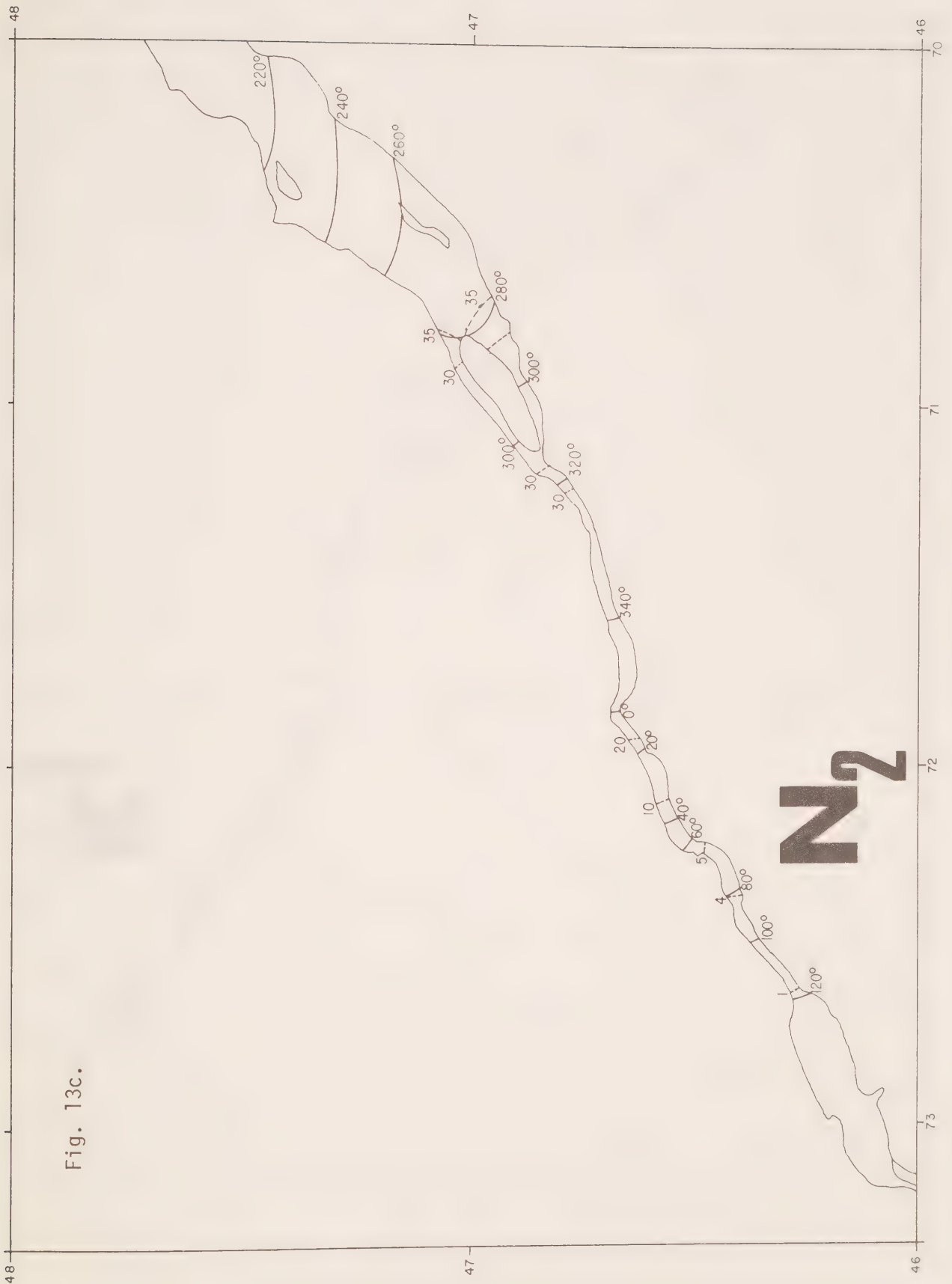
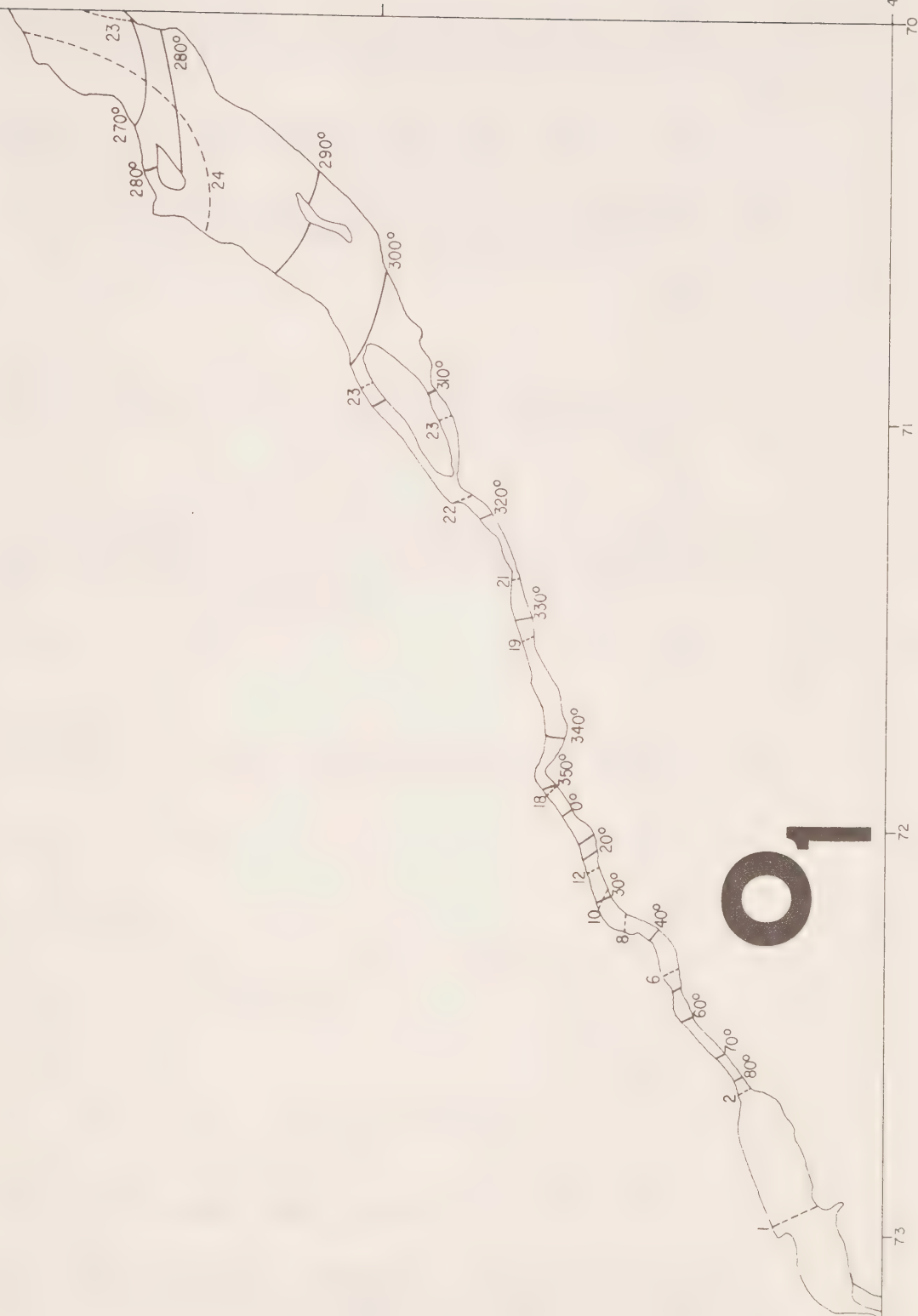


Fig. 13d.



Fig. 13e.



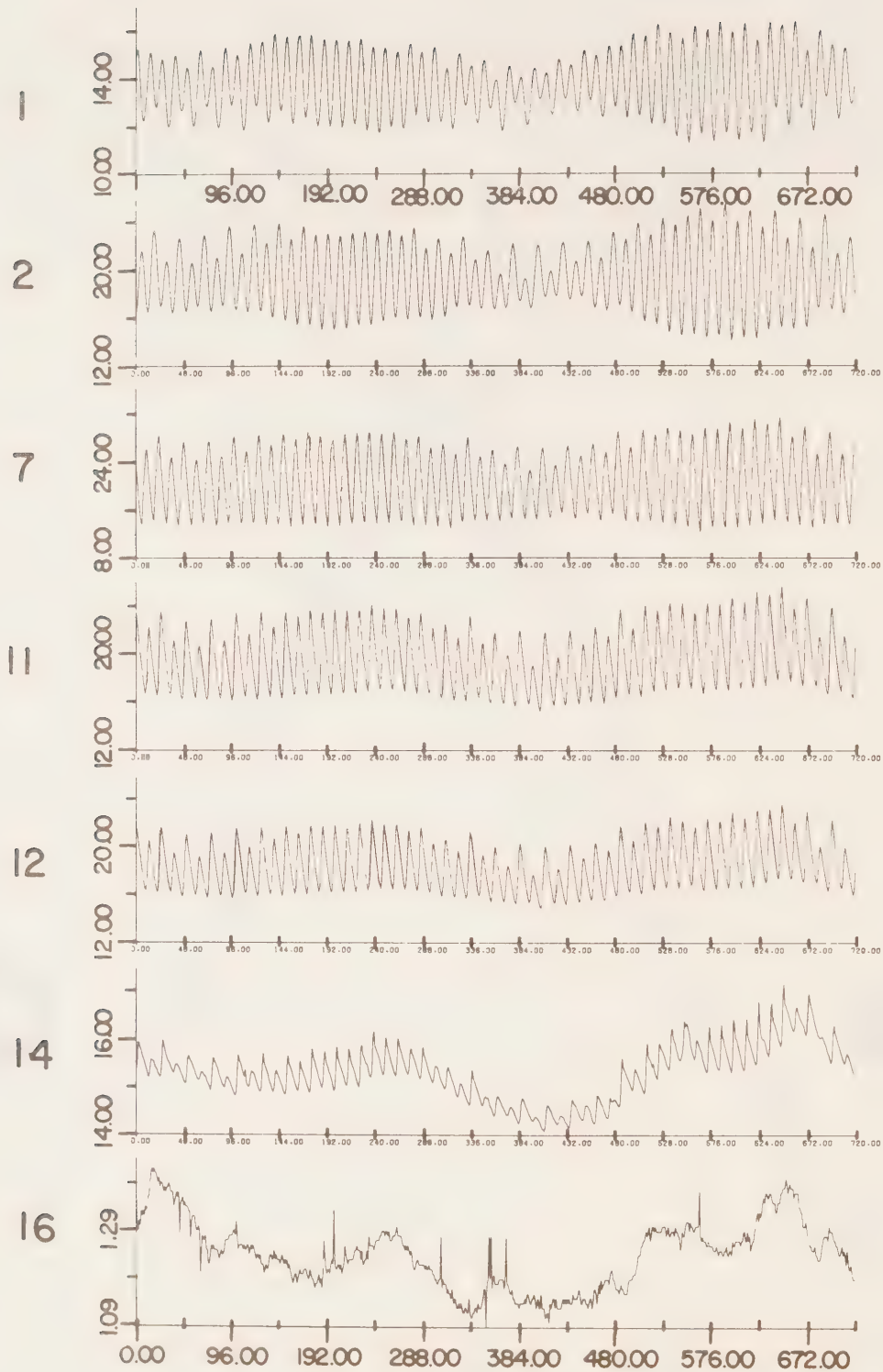


Fig. 14. Creation of a semimonthly tide in the upper reaches of the St. Lawrence River caused by the succession of spring and neap tides downstream (from Godin 1979).

Fig. 15. Tidal pattern around the Gulf of St. Lawrence and the upper estuary of the St. Lawrence River. (a) Gulf of St. Lawrence (b) Upper estuary.

Fig. 15a.

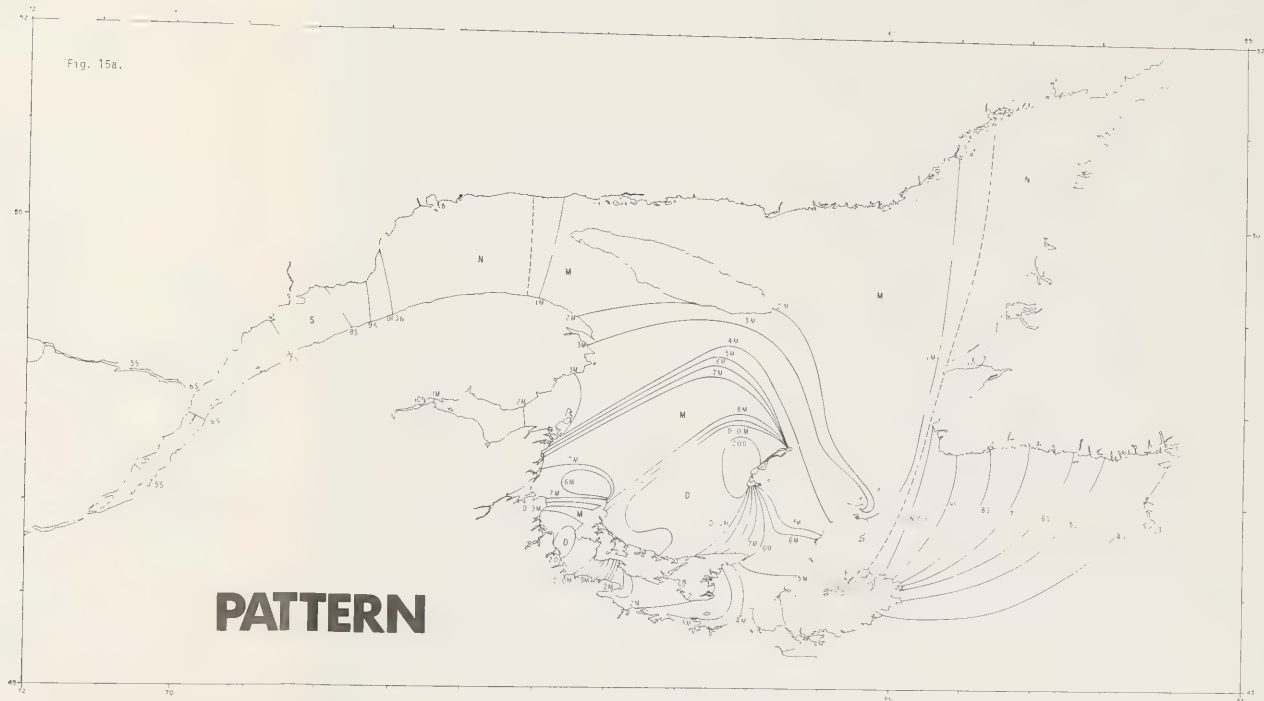


Fig. 15b.



normal category to finally assume a semidiurnal character past Pointe des Monts. It is semidiurnal inside the St. Lawrence River, but as the semidiurnal signal gets damped more rapidly than the diurnal it gradually acquires a stronger diurnal inequality.

7.3 Bay of Fundy

Although this area is world famous the actual data we possess about the tide over the body of the Bay of Fundy is quite inadequate. This results exactly from the fact that large tides imply foreshores that dry for miles and ranges which tax most instruments. The charts which we present (Fig. 16) should be considered as schematic at best. The wave from the Gulf of Maine divides and its eastern branch enters the Bay of Fundy. There seems to be some diffraction around Grand Manan Island.

Inspection of the charts for M_2 , S_2 and N_2 (Fig. 16a, b, c) indicates that N_2 is the true resonating semidiurnal constituent in the Bay of Fundy. The N_2 tide is almost simultaneous over the whole bay and its amplitude increases threefold between Grand Manan and Cape d'Or. In contrast M_2 only doubles over the same stretch and S_2 less than doubles; M_2 takes $1/2$ hour to reach Cape d'Or and S_2 about an hour. The largest amplitudes are found inside Minas and Cumberland Basin in which submerged gauges were deployed, thus increasing the quality of the information. The tide takes nearly an hour to penetrate Minas Basin in which it is further amplified. This time M_2 seems more favored because it increases a further 50% while N_2 gains a mere 10%.

The diurnal tide (Fig. 16d, e) is similar in profile to the semidiurnal tide except that it falls far away from resonance and is little amplified in the upper regions of the bay.

8. USE OF COTIDAL CHARTS FOR PREDICTION

The contributions of the five constituents illustrated in the charts, in conjunction with P_1 and K_2 , usually amount to over 90% of the tide observed; therefore they can be used to prepare predictions of the tide whenever a high degree of precision is not necessary, or at points in the ocean where the tide has never been observed. The cotidal charts represent an intelligent extrapolation of the information available and although they may be deficient in some details, they constitute the best guess as to what is happening.

Should a prediction be required at an ungauged site, its position is located on the charts and the corresponding values of M_2 , S_2 , N_2 , K_1 and O_1 are obtained by interpolation between the cotidal lines. The additional values of P_1 and K_2 are inferred by using the regional values of r and ϕ and applying them to K_1 and S_2 . Then it must be decided in which time zone the prediction is to be made since the charts are in Greenwich time. In a scientific application it is preferable to retain the Greenwich time because the switch to other time zones is an unending source of error and confusion. If there is reason to prefer to work in some other time zone, the Greenwich



Fig. 16. Cotidal charts for the constituents M_2 , S_2 , N_2 , K_1 and O_1 in the Bay of Fundy. (a) M_2 (b) S_2 (c) N_2 (d) K_1 (e) O_1 .



Fig. 16b.



Fig. 16c.

Fig. 16d.

Fig. 16e.

phase lags of the constituents have to be first transformed to the chosen time zone with the help of transformation (4). At this stage we are provided with a set of amplitude and phase (A, g) for the seven constituents mentioned. This is not sufficient. We also need the astronomical argument V of the constituent, which is derived from astronomical knowledge and the nodal corrections (f, u) derived from tidal theory, which modify the amplitude A and the argument V of each constituent. In addition, although we always write a cosine in (1) for the contribution of all constituents, theory informs us that diurnal constituents actually enter as sines, while semi-diurnal constituents contribute as cosines. In addition their contribution may be positive or negative, and this additional information is also provided by theory.

The calculation of angles, when there is a possibility that we will be consistently faced with angles containing very large multiples of 360° , is usually done with the help of a special angular unit called "cycles". An angle is measured by the portion of a complete circle it covers; therefore one cycle corresponds to a full circle or 360° in degree measure or 2π radians in radian measure. Thus 45° in cycles becomes:

$$45/360 = 1/8 = .125 \text{ cycle}$$

The advantage of cycle measure is that if we had to multiply 45° by 75, we obtain 3375° which has to be reduced to 135° . The same calculation in cycles becomes:

$$75 \times .125 = 9.375 \text{ cycle} = .375 \text{ cycle } (135^\circ)$$

The reduction is done simply by dropping any whole number of cycles in the final result since whole cycles represent complete turns around the circle. Henceforth we shall use cycles in the elaboration of formulas for predictions with the understanding that the argument of the sine or cosine is expressed in degrees or radians in the ultimate step.

As an example we set up a scheme of predictions for Churchill starting at 00 hour (Central Standard Time) June 5, 1980. In order to do this we need two additional tables: one giving the number of days elapsed since the beginning of the year (Table 4), the other the astronomical argument V of each constituent at 00 hours GMT at the beginning of the year and the mean nodal corrections (f, u) for that (Table 5) year. The latter tables were prepared by the German Hydrographic Institute and cover the years 1900-1999 (Anon. 1967). Table 4 indicates that June 5 is the 157th day of 1980, a leap year. Table 5 gives the argument V for January 1 at 00 hour; we therefore have to increase it by adding the number of hours elapsed between January 1 and June 5 multiplied by the angular speed of the constituent in order to adjust to the initial time of the prediction. The table actually gives $V_0 + u$, i.e. automatically incorporating the nodal correction, so we simply add the adjustment to $V_0 + u$ to get $V + u$ at the desired date. Then one multiplies the amplitude A by f in order to obtain the adjusted amplitude of the constituent during the interval of predictions.

Table 4. Number of days elapsed since the beginning of the year (from Godin 1972, p. 16).

<i>mm</i>	Month	Number of days	Number of days elapsed in the year at the beginning of the month
01	January	31	000
02	February	28 (29)	031
03	March	31	059 (060)
04	April	30	090 (091)
05	May	31	120 (121)
06	June	30	151 (152)
07	July	31	181 (182)
08	August	31	212 (213)
09	September	30	243 (244)
10	October	31	273 (274)
11	November	30	304 (305)
12	December	31	334 (335)

Table 6 shows this task of preparation for Churchill. The z_0 in the formula, e.g. (1) and Table 6, stands for the reference level. It is usually unknown in unexplored areas and is then replaced by zero, so that the predictions are about mean sea level. If one wants to obtain the hourly predicted levels, t is increased by increments of 1 hour. If the time and height of high and low water are desired, one looks for the zeros of the derivative of $z(t)$; a practical scheme for such a search could be the one suggested by Godin and Taylor (1973). The map of patterns indicates if the local tide will be of semidiurnal, mixed or diurnal character.

9. ACKNOWLEDGMENTS

The charts for M_2 and K_1 were updated in the area east of Prince of Wales Island thanks to additional data acquired with the help of submerged gauges installed by the Tidal Sections of the eastern and western regions. The cotidal charts were drawn in Ensenada, B.C. by Sergio A. Ramos Rodriguez, Pedro Leonardo Villaseñor Jimenez and Patricia Hernandez Muñoz at the Centro de Investigacion Cientifica y de Educacion Superior de Ensenada (CICESE). I wish to thank the Direction of this Institute for its benevolent support which has made this publication possible. I wish to thank in particular Dr. Saul Borrego, Director General and Ing. Marco Uribe, Director, Oceanography and also to express appreciation to Mrs. Margaret K. Johnstone for the preparation and typing of this manuscript.

Table 5. Tables of f and $V_0 + u$ between 1900 and 1999 for O_1 , P_1 , K_1 , N_2 , M_2 , S_2 and K_2 from tables prepared by the German Hydrographic Institute (Anon. 1967).

	f	u	$V_0 + u$		f	u	$V_0 + u$
1900	0.950	-010.88	345.3	1950	1.183	+000.04	061.4
01	0.893	-009.99	087.1	51	1.183	-002.48	150.8
02	0.847	-006.99	191.1	52	1.154	-004.91	258.4
03	0.815	-002.50	296.6	53	1.112	-007.67	331.3
04	0.806	+002.19	042.3	54	1.068	-009.94	070.0
05	0.830	+006.07	121.8	55	1.015	-010.82	170.1
06	0.884	+008.91	225.6	56	0.948	-010.43	271.5
07	0.949	+010.71	328.4	57	0.880	-009.11	348.4
08	1.009	+011.08	069.8	58	0.832	-006.54	092.0
09	1.061	+009.74	144.1	59	0.812	-002.38	197.1
1910	1.115	+007.43	242.8	1960	0.816	+002.72	303.2
11	1.160	+005.17	341.5	61	0.842	+007.15	023.3
12	1.179	+002.87	080.2	62	0.887	+009.72	126.9
13	1.176	-000.11	152.8	63	0.951	+010.53	228.7
14	1.169	-003.41	250.5	64	1.022	+010.41	329.5
15	1.153	-006.03	348.9	65	1.081	+009.61	044.3
16	1.112	-007.93	088.0	66	1.120	+007.65	143.4
17	1.052	-009.69	161.8	67	1.153	+004.71	241.4
18	0.990	-011.03	261.5	68	1.181	+001.83	339.5
19	0.933	-010.86	002.7	69	1.188	-000.61	052.7
1920	0.877	-008.69	105.8	1970	1.167	-003.28	151.1
21	0.828	-005.09	185.0	71	1.136	-006.34	249.0
22	0.803	-000.87	290.3	72	1.102	-008.82	347.5
23	0.813	+003.40	035.5	73	1.053	-010.10	061.8
24	0.854	+007.30	140.4	74	0.985	-010.55	162.4
25	0.910	+010.15	218.9	75	0.915	-010.32	263.6
26	0.967	+011.21	320.9	76	0.862	-008.66	006.3
27	1.026	+010.40	061.1	77	0.827	-004.98	085.6
28	1.088	+008.66	160.4	78	0.811	-000.01	191.5
29	1.139	+006.83	234.2	79	0.818	+004.72	297.2
1930	1.167	+004.61	332.9	1980	0.854	+008.03	041.5
31	1.177	+001.54	070.9	81	0.914	+009.91	119.0
32	1.178	-001.72	168.6	82	0.984	+010.79	220.9
33	1.171	-004.31	241.6	83	1.044	+010.57	321.7
34	1.136	-006.48	340.5	84	1.090	+008.86	061.0
35	1.084	-008.79	079.1	85	1.135	+006.19	133.9
36	1.030	-010.70	178.2	86	1.173	+003.63	232.4
37	0.975	-011.10	253.4	87	1.186	+001.26	331.0
38	0.911	-009.83	355.7	88	1.174	-001.62	069.1
39	0.850	-007.34	099.2	89	1.156	-004.86	141.5
1940	0.812	-003.88	203.6	1990	1.132	-007.43	239.9
41	0.807	+000.51	283.6	91	1.086	-009.05	339.3
42	0.831	+005.20	029.3	92	1.021	-010.26	079.1
43	0.874	+008.97	134.1	93	0.954	-010.95	154.0
44	0.926	+010.78	236.9	94	0.898	-010.11	255.8
45	0.988	+010.67	312.4	95	0.850	-007.17	354.8
46	1.057	+009.67	052.4	96	0.815	-002.76	105.2
47	1.113	+008.34	152.1	97	0.805	+001.85	185.4
48	1.145	+006.22	250.9	98	0.828	+005.77	290.3
49	1.165	+003.15	323.5	99	0.881	+008.77	034.3

$O_1 = 145.555$

Table 5. (Contd.)

	f	u	$V_0 + u$		f	u	$V_0 + u$
1900	1.003	+000.66	350.5	1950	0.990	-000.09	349.8
01	1.007	+000.48	350.5	51	0.992	+000.18	350.3
02	1.012	+000.34	350.6	52	0.992	+000.43	350.8
03	1.013	+000.22	350.7	53	0.993	+000.53	350.2
04	1.012	-000.03	350.7	54	0.996	+000.55	350.4
05	1.010	-000.36	349.7	55	1.002	+000.62	350.7
06	1.009	-000.56	349.7	56	1.006	+000.69	351.1
07	1.006	-000.58	349.9	57	1.007	+000.59	350.2
08	1.001	-000.56	350.2	58	1.010	+000.31	350.2
09	0.996	-000.59	349.4	59	1.013	+000.05	350.1
1910	0.994	-000.56	349.7	1960	1.014	-000.11	350.2
11	0.993	-000.35	350.1	61	1.011	-000.27	349.3
12	0.991	-000.08	350.6	62	1.006	-000.51	349.3
13	0.989	+000.08	350.0	63	1.004	-000.69	349.4
14	0.990	+000.16	350.4	64	1.001	-000.66	349.6
15	0.993	+000.33	350.8	65	0.997	-000.51	349.0
16	0.996	+000.58	351.2	66	0.993	-000.41	349.4
17	0.997	+000.71	350.6	67	0.991	-000.36	349.7
18	1.000	+000.65	350.8	68	0.991	-000.19	350.1
19	1.006	+000.54	350.9	69	0.991	+000.10	349.6
1920	1.010	+000.49	351.1	1970	0.990	+000.33	350.1
21	1.012	+000.37	350.3	71	0.991	+000.41	350.4
22	1.011	+000.09	350.2	72	0.995	+000.48	350.7
23	1.011	-000.24	350.1	73	1.000	+000.63	350.1
24	1.011	-000.44	350.2	74	1.003	+000.74	350.5
25	1.008	-000.49	349.4	75	1.005	+000.64	350.6
26	1.002	-000.56	349.5	76	1.009	+000.40	350.6
27	0.998	-000.66	349.7	77	1.013	+000.21	349.7
28	0.996	-000.63	350.0	78	1.014	+000.07	349.8
29	0.994	-000.42	349.4	79	1.011	-000.15	349.8
1930	0.991	-000.19	349.9	1980	1.008	-000.45	349.7
31	0.989	-000.07	350.2	81	1.007	-000.64	349.8
32	0.990	+000.03	350.6	82	1.004	-000.63	349.0
33	0.992	+000.26	350.1	83	0.999	-000.54	349.4
34	0.994	+000.52	350.6	84	0.994	-000.52	349.6
35	0.995	+000.63	350.9	85	0.992	-000.48	348.9
36	0.998	+000.61	351.1	86	0.992	-000.22	349.4
37	1.004	+000.59	350.4	87	0.991	+000.01	349.9
38	1.008	+000.61	350.6	88	0.989	+000.20	350.3
39	1.010	+000.50	350.7	89	0.990	+000.28	349.6
1940	1.011	+000.21	350.7	1990	0.994	+000.41	350.0
41	1.013	-000.11	349.6	91	0.998	+000.62	350.5
42	1.013	-000.28	349.7	92	1.000	+000.71	350.8
43	1.010	-000.39	349.8	93	1.002	+000.65	350.0
44	1.004	-000.55	349.9	94	1.007	+000.48	350.1
45	1.001	-000.70	349.0	95	1.012	+000.27	350.2
46	0.999	-000.66	349.3	96	1.013	+000.24	350.3
47	0.996	-000.47	349.7	97	1.011	-000.02	349.3
48	0.992	-000.30	350.1	98	1.010	-000.35	349.2
49	0.989	-000.22	349.5	99	1.009	-000.55	349.2

 $P_1 = 163.555$

Table 5. (Contd.)

	f	u	$V_o + u$		f	u	$V_o + u$
1900	0.973	+008.66	018.8	1950	1.112	-000.33	009.8
01	0.935	+007.46	017.4	51	1.109	+002.24	012.1
02	0.904	+005.19	014.9	52	1.096	+004.64	014.2
03	0.885	+002.07	011.5	53	1.073	+006.67	017.0
04	0.884	-001.42	007.8	54	1.043	+008.14	018.3
05	0.899	-004.65	005.3	55	1.006	+008.83	018.7
06	0.928	-007.11	002.6	56	0.967	+008.54	018.2
07	0.966	-008.52	001.0	57	0.929	+007.16	017.5
08	1.005	-008.83	000.4	58	0.900	+004.73	014.9
09	1.042	-008.17	001.8	59	0.884	+001.51	011.4
1910	1.073	-006.72	003.1	1960	0.885	-001.97	007.7
11	1.095	-004.70	004.8	61	0.903	-005.11	005.3
12	1.108	-002.31	007.0	62	0.934	-007.41	002.8
13	1.112	+000.26	010.3	63	0.972	-008.64	001.3
14	1.106	+002.80	012.6	64	1.011	-008.79	000.9
15	1.091	+005.13	014.7	65	1.047	-007.98	002.5
16	1.067	+007.06	016.4	66	1.077	-006.43	003.8
17	1.035	+008.37	018.4	67	1.098	-004.33	005.6
18	0.997	+008.86	018.7	68	1.110	-001.90	007.8
19	0.958	+008.33	017.9	69	1.112	+000.67	011.1
1920	0.922	+006.70	016.1	1970	1.105	+003.20	013.4
21	0.895	+004.05	014.2	71	1.088	+005.48	015.5
22	0.883	+000.73	010.6	72	1.063	+007.32	017.1
23	0.888	-002.73	006.9	73	1.029	+008.51	019.0
24	0.909	-005.72	003.7	74	0.991	+008.84	019.1
25	0.942	-007.79	002.3	75	0.952	+008.14	018.2
26	0.981	-008.77	001.1	76	0.916	+006.34	016.1
27	1.020	-008.68	001.0	77	0.892	+003.55	014.1
28	1.055	-007.69	001.7	78	0.882	+000.16	010.5
29	1.082	-005.99	004.2	79	0.890	-003.26	006.8
1930	1.101	-003.81	006.1	1980	0.914	-006.12	003.7
31	1.111	-001.33	008.4	81	0.948	-008.02	002.5
32	1.111	+001.25	010.7	82	0.987	-008.82	001.5
33	1.102	+003.74	013.9	83	1.026	-008.58	001.5
34	1.083	+005.94	015.9	84	1.060	-007.46	002.4
35	1.056	+007.65	017.4	85	1.086	-005.67	004.9
36	1.021	+008.67	018.1	86	1.104	-003.42	006.9
37	0.982	+008.78	019.0	87	1.112	-000.91	009.2
38	0.943	+007.83	017.8	88	1.110	+001.67	011.5
39	0.910	+005.79	015.5	89	1.099	+004.12	014.7
1940	0.888	+002.82	012.3	1990	1.079	+006.26	016.6
41	0.882	-000.63	009.6	91	1.050	+007.87	018.0
42	0.894	-003.97	006.0	92	1.015	+008.75	018.7
43	0.921	-006.64	003.1	93	0.976	+008.70	019.4
44	0.957	-008.30	001.2	94	0.937	+007.57	018.0
45	0.996	-008.85	001.4	95	0.905	+005.36	015.5
46	1.034	-008.40	001.7	96	0.886	+002.28	012.2
47	1.066	-007.11	002.7	97	0.883	-001.20	009.5
48	1.091	-005.19	004.4	98	0.898	-004.46	006.0
49	1.106	-002.87	007.5	99	0.926	-006.98	003.2

Table 5. (Contd.)

	f	u	$v_o + u$		f	u	$v_o + u$
1900	1.016	+001.83	065.5	1950	0.964	+000.12	216.0
01	1.021	+001.47	077.2	51	0.968	+000.55	228.5
02	1.031	+001.20	089.0	52	0.968	+001.20	241.1
03	1.038	+000.34	100.1	53	0.980	+001.92	216.4
04	1.034	-000.33	111.5	54	0.993	+001.93	228.5
05	1.033	-000.73	085.7	55	1.000	+002.02	240.6
06	1.029	-001.55	096.9	56	1.015	+002.10	252.7
07	1.014	-001.99	108.5	57	1.028	+001.46	226.7
08	1.004	-001.97	120.5	58	1.030	+000.93	238.2
09	0.994	-002.20	094.9	59	1.037	+000.50	249.8
1910	0.977	-001.93	107.2	1960	1.040	-000.48	260.8
11	0.970	-001.15	120.0	61	1.030	-001.14	234.7
12	0.967	-000.73	132.4	62	1.025	-001.46	246.5
13	0.960	+000.03	107.8	63	1.016	-002.09	257.9
14	0.966	+001.02	120.8	64	0.998	-002.22	269.8
15	0.975	+001.35	133.2	65	0.989	-001.86	244.7
16	0.980	+001.79	145.6	66	0.980	-001.79	256.8
17	0.995	+002.24	120.7	67	0.967	-001.25	269.4
18	1.009	+001.95	132.4	68	0.965	-000.34	282.3
19	1.015	+001.73	144.2	69	0.966	+000.09	257.3
1920	1.027	+001.56	156.1	1970	0.964	+000.80	270.1
21	1.036	+000.75	129.9	71	0.974	+001.64	282.9
22	1.034	+000.11	141.2	72	0.986	+001.78	295.1
23	1.036	-000.34	152.8	73	0.992	+002.04	269.9
24	1.034	-001.23	164.0	74	1.008	+002.25	282.2
25	1.020	-001.77	138.0	75	1.022	+001.73	293.7
26	1.012	-001.88	149.9	76	1.026	+001.29	305.3
27	1.002	-002.26	161.6	77	1.036	+000.90	279.5
28	0.984	-002.12	173.8	78	1.040	-000.07	290.5
29	0.975	-001.46	149.0	79	1.033	-000.75	301.9
1930	0.970	-001.14	161.4	1980	1.030	-001.14	313.5
31	0.961	-000.42	174.1	81	1.023	-001.88	287.4
32	0.964	+000.58	187.1	82	1.006	-002.13	299.2
33	0.971	+000.98	162.1	83	0.996	-001.93	311.4
34	0.974	+001.53	174.7	84	0.987	-002.01	323.3
35	0.987	+002.12	187.3	85	0.972	-001.59	298.4
36	1.001	+001.98	199.2	86	0.968	-000.77	311.2
37	1.008	+001.92	173.7	87	0.966	-000.37	323.6
38	1.021	+001.86	185.7	88	0.962	+000.37	336.4
39	1.032	+001.13	197.0	89	0.969	+001.29	311.9
1940	1.033	+000.53	208.4	1990	0.979	+001.56	324.2
41	1.038	+000.08	182.6	91	0.985	+001.96	336.6
42	1.038	-000.87	193.7	92	1.000	+002.32	349.0
43	1.026	-001.48	205.1	93	1.015	+001.92	323.2
44	1.019	-001.71	216.9	94	1.021	+001.60	334.9
45	1.009	-002.22	191.0	95	1.033	+001.28	346.6
46	0.991	-002.22	203.0	96	1.039	+000.34	357.7
47	0.982	-001.71	215.5	97	1.035	-000.34	331.6
48	0.974	-001.50	227.8	98	1.034	-000.78	343.2
49	0.963	-000.85	203.0	99	1.028	-001.60	354.4

Table 5. (Contd.)

	f	u	$V_0 + u$		f	u	$V_0 + u$
1900	1.014	+001.99	008.3	1950	0.963	-000.05	071.4
01	1.024	+001.65	108.7	51	0.964	+000.62	172.8
02	1.032	+001.09	208.9	52	0.970	+001.23	274.1
03	1.037	+000.40	309.0	53	0.980	+001.76	351.0
04	1.038	-000.30	049.0	54	0.991	+002.09	092.1
05	1.034	-000.95	124.8	55	1.002	+002.13	192.9
06	1.026	-001.51	225.0	56	1.015	+001.92	293.5
07	1.015	-001.93	325.3	57	1.026	+001.53	009.5
08	1.003	-002.15	065.8	58	1.034	+000.99	109.7
09	0.991	-002.07	142.3	59	1.037	+000.33	209.8
1910	0.980	-001.74	243.4	1960	1.037	-000.40	309.8
11	0.970	-001.27	344.6	61	1.032	-001.09	025.5
12	0.965	-000.68	085.9	62	1.025	-001.62	125.7
13	0.964	+000.05	163.0	63	1.014	-001.95	226.1
14	0.966	+000.81	264.5	64	1.001	-002.10	326.7
15	0.972	+001.42	005.9	65	0.989	-002.06	043.1
16	0.981	+001.82	107.1	66	0.978	-001.74	144.2
17	0.994	+002.07	183.7	67	0.970	-001.16	245.5
18	1.006	+002.12	284.5	68	0.964	-000.49	346.9
19	1.017	+001.89	025.0	69	0.963	+000.17	064.0
1920	1.027	+001.43	125.3	1970	0.967	+000.85	165.4
21	1.035	+000.81	201.1	71	0.974	+001.49	266.8
22	1.038	+000.14	301.1	72	0.983	+001.94	008.0
23	1.036	-000.54	041.2	73	0.995	+002.11	084.6
24	1.031	-001.18	141.3	74	1.008	+002.05	185.2
25	1.022	-001.72	217.2	75	1.020	+001.81	285.8
26	1.011	-002.06	317.6	76	1.029	+001.37	026.1
27	0.999	-002.12	058.3	77	1.035	+000.74	101.8
28	0.986	-001.94	159.2	78	1.037	+000.02	201.8
29	0.975	-001.60	235.9	79	1.036	-000.69	301.9
1930	0.968	-001.09	337.2	1980	1.030	-001.29	042.0
31	0.965	-000.38	078.6	81	1.020	-001.75	118.0
32	0.964	+000.39	180.2	82	1.008	-002.05	218.4
33	0.967	+001.05	257.2	83	0.996	-002.15	319.1
34	0.975	+001.56	358.4	84	0.985	-001.95	060.0
35	0.987	+001.95	099.6	85	0.975	-001.49	136.8
36	0.998	+002.15	200.5	86	0.967	-000.92	238.2
37	1.010	+002.06	276.8	87	0.963	-000.29	339.6
38	1.021	+001.71	017.2	88	0.965	+000.43	021.0
39	1.031	+001.20	117.5	89	0.969	+001.16	158.1
1940	1.037	+000.58	217.6	1990	0.977	+001.70	259.4
41	1.038	-000.11	293.3	91	0.987	+001.99	060.5
42	1.034	-000.81	033.3	92	1.000	+002.10	101.3
43	1.028	-001.44	133.5	93	1.013	+002.01	177.6
44	1.018	-001.88	233.8	94	1.023	+001.68	278.0
45	1.007	-002.08	309.9	95	1.031	+001.12	018.2
46	0.993	-002.07	050.7	96	1.037	+000.45	118.3
47	0.981	-001.87	151.7	97	1.038	-000.25	141.0
48	0.973	-001.45	252.8	98	1.034	-000.91	294.1
49	0.967	-000.79	329.9	99	1.026	-001.48	041.3

Table 5. (Contd.)

	f	u	$V_0 + u$		f	u	$V_0 + u$
1900	0.999	-000.12	359.9	1950	1.002	+000.01	000.0
01	0.999	-000.10	359.9	51	1.002	-000.04	000.0
02	0.998	-000.06	359.9	52	1.002	-000.07	359.9
03	0.998	-000.03	000.0	53	1.001	-000.10	359.9
04	0.998	+000.02	000.0	54	1.001	-000.12	359.9
05	0.998	+000.06	000.1	55	1.000	-000.13	359.9
06	0.998	+000.09	000.1	56	0.999	-000.12	359.9
07	0.999	+000.12	000.1	57	0.999	-000.09	359.9
08	1.000	+000.13	000.1	58	0.998	-000.06	359.9
09	1.001	+000.12	000.1	59	0.998	-000.02	000.0
1910	1.001	+000.10	000.1	1960	0.998	+000.02	000.0
11	1.002	+000.08	000.1	61	0.998	+000.06	000.1
12	1.002	+000.04	000.0	62	0.999	+000.10	000.1
13	1.002	000.00	000.0	63	0.999	+000.12	000.1
14	1.002	-000.05	000.0	64	1.000	+000.13	000.1
15	1.002	-000.08	359.9	65	1.001	+000.12	000.1
16	1.001	-000.11	359.9	66	1.001	+000.10	000.1
17	1.000	-000.12	359.9	67	1.002	+000.07	000.1
18	1.000	-000.13	359.9	68	1.002	+000.03	000.0
19	0.999	-000.11	359.9	69	1.002	-000.01	000.0
1920	0.998	-000.09	359.9	1970	1.002	-000.05	359.9
21	0.998	-000.05	359.9	71	1.002	-000.09	359.9
22	0.998	-000.01	000.0	72	1.001	-000.11	359.9
23	0.998	+000.03	000.0	73	1.000	-000.13	359.9
24	0.998	+000.07	000.1	74	1.000	-000.12	359.9
25	0.999	+000.10	000.1	75	0.999	-000.11	359.9
26	0.999	+000.12	000.1	76	0.998	-000.08	359.9
27	1.000	+000.13	000.1	77	0.998	-000.04	000.0
28	1.001	+000.12	000.1	78	0.998	000.00	000.0
29	1.001	+000.09	000.1	79	0.998	+000.04	000.0
1930	1.002	+000.06	000.1	1980	0.998	+000.08	000.1
31	1.002	+000.02	000.0	81	0.999	+000.11	000.1
32	1.002	-000.02	000.0	82	0.999	+000.12	000.1
33	1.002	-000.06	359.9	83	1.000	+000.13	000.1
34	1.001	-000.09	359.9	84	1.001	+000.11	000.1
35	1.001	-000.12	359.9	85	1.002	+000.09	000.1
36	1.000	-000.13	359.9	86	1.002	+000.06	000.1
37	0.999	-000.12	359.9	87	1.002	+000.02	000.0
38	0.999	-000.10	359.9	88	1.002	-000.03	000.0
39	0.998	-000.07	359.9	89	1.002	-000.07	359.9
1940	0.998	-000.03	000.0	1990	1.001	-000.10	359.9
41	0.998	+000.01	000.0	91	1.001	-000.12	359.9
42	0.998	+000.05	000.0	92	1.000	-000.13	359.9
43	0.998	+000.09	000.1	93	0.999	-000.12	359.9
44	0.999	+000.11	000.1	94	0.999	-000.10	359.9
45	1.000	+000.12	000.1	95	0.998	-000.07	359.9
46	1.000	+000.12	000.1	96	0.998	-000.03	000.0
47	1.001	+000.11	000.1	97	0.998	+000.01	000.0
48	1.002	+000.08	000.1	98	0.998	+000.06	000.1
49	1.002	+000.05	000.0	99	0.998	+000.09	000.1

 $S_2 = 273.555$

Table 5. (Concluded)

	f	u	$V_0 + u$		f	u	$V_0 + u$
1900	0.917	+017.02	217.4	1950	1.315	-000.69	199.5
01	0.838	+014.22	214.1	51	1.302	+004.73	204.4
02	0.783	+009.59	209.0	52	1.256	+009.75	209.0
03	0.753	+003.75	202.7	53	1.183	+013.90	214.6
04	0.751	-002.56	195.9	54	1.092	+016.71	216.9
05	0.775	-008.56	191.4	55	0.995	+017.75	217.5
06	0.826	-013.47	186.0	56	0.903	+016.71	216.0
07	0.901	-016.65	182.4	57	0.828	+013.58	214.3
08	0.992	-017.75	180.8	58	0.776	+008.71	209.0
09	1.090	-016.76	183.3	59	0.751	+002.74	202.5
1910	1.181	-014.00	185.5	1960	0.753	-003.57	195.8
11	1.255	-009.88	189.2	61	0.782	-009.44	191.4
12	1.301	-004.88	193.7	62	0.837	-014.11	186.2
13	1.315	+000.55	200.6	63	0.915	-016.97	182.9
14	1.294	+005.92	205.5	64	1.008	-017.72	181.7
15	1.242	+010.78	209.9	65	1.105	-016.43	184.5
16	1.164	+014.67	213.3	66	1.194	-013.41	187.0
17	1.070	+017.11	217.3	67	1.264	-009.12	190.8
18	0.973	+017.70	217.4	68	1.306	-004.02	195.4
19	0.884	+016.18	215.4	69	1.314	+001.43	202.4
1920	0.814	+012.62	211.3	1970	1.288	+006.75	207.2
21	0.768	+007.43	207.6	71	1.231	+011.48	211.5
22	0.749	+001.31	201.0	72	1.150	+015.17	214.7
23	0.757	-004.96	194.3	73	1.055	+017.34	218.4
24	0.792	-010.63	188.2	74	0.958	+017.60	218.1
25	0.853	-014.94	185.3	75	0.872	+015.74	215.8
26	0.935	-017.33	182.5	76	0.805	+011.87	211.4
27	1.030	-017.60	181.7	77	0.763	+006.48	207.6
28	1.127	-015.88	183.0	78	0.748	+000.29	200.9
29	1.212	-012.54	187.8	79	0.761	-005.93	194.2
1930	1.276	-008.02	191.8	1980	0.800	-011.43	188.2
31	1.311	-002.81	196.6	81	0.865	-015.46	185.7
32	1.311	+002.65	201.6	82	0.950	-017.52	183.1
33	1.278	+007.89	208.3	83	1.046	-017.45	182.7
34	1.214	+012.43	212.3	84	1.141	-015.44	184.3
35	1.129	+015.81	215.2	85	1.224	-011.87	189.3
36	1.033	+017.58	216.5	86	1.284	-007.21	193.5
37	0.937	+017.37	217.8	87	1.313	-001.93	198.3
38	0.854	+015.03	215.0	88	1.308	+003.52	203.3
39	0.793	+010.77	210.3	89	1.269	+008.68	209.9
1940	0.757	+005.13	204.2	1990	1.202	+013.06	213.8
41	0.749	-001.14	199.4	91	1.114	+016.21	216.5
42	0.767	-007.27	192.8	92	1.017	+017.69	217.5
43	0.812	-012.49	187.1	93	0.923	+017.13	218.4
44	0.882	-016.11	183.0	94	0.843	+014.46	215.3
45	0.971	-017.69	182.9	95	0.786	+009.94	210.3
46	1.068	-017.15	182.9	96	0.754	+004.14	204.0
47	1.162	-014.76	184.9	97	0.750	-002.16	199.2
48	1.240	-010.90	188.2	98	0.773	-008.19	192.7
49	1.293	-006.05	194.6	99	0.822	-013.20	187.2

Table 6. Preparation of data for the predictions at Churchill.

Constituent	Amplitude A cm	Greenwich phase lag g deg	Astronomical argument V-u 1980 deg	Node correction f cm	Adjusted amplitude fA cm	Initial argument V-u-g cycles	Initial Function to be used
		Central Time(Z=6) cycles	Jan 1 Adjustment Jun 5 cycles				
O ₁	4	166 .46111	41.5	.854	3	.5913	sine
P ₁	2	215 .59722	349.7	1.008	2	.9443	sine
K ₁	8	218 .60556	3.7	.914	7	.8346	-sine
M ₂	30	179 .49722	313.5	1.030	31	.0428	cosine
M ₂	154	211 .58611	42.0	1.030	159	.8975	cosine
S ₂	47	274 .76111	.1	.998	47	.2389	cosine
K ₂	13	272 .75555	188.2	.800	10	.6269	cosine
			.52278 .85969 .38247				

Formula for the predictions:

$$\begin{aligned}
 z(t) = & z_0 \text{ (the reference level, which may be mean sea level, or datum, or arbitrary gauge zero)} \\
 & + 3 \sin (.5913+.038713t) \text{ constituent O}_1 \\
 & + 2 \sin (.9443+.041553t) \text{ P}_1 \\
 & - 7 \sin (.8346+.041781t) \text{ K}_1 \\
 & + 31 \cos (.0428+.078999t) \text{ N}_2 \\
 & + 159 \cos (.8975+.080511t) \text{ M}_2 \\
 & + 47 \cos (.2389+.083333t) \text{ S}_2 \\
 & + 10 \cos (.6269+.083561t) \text{ K}_2 \\
 & \text{cm} \qquad \qquad \qquad \text{units of predicted level}
 \end{aligned}$$

t = 0 in the formula corresponds to 00 hours June 5, 1980 (Z = +6 Central Standard Time) which has been used to calculate the astronomical arguments V at t = 0. The times of high and low water are found by searching for the zeros of z'(t) = .11619 cos (.5913+.038731t) + .08311 cos (.9443+.041553t) - .29247 cos (.8346+.041781t) - 2.44897 sin (.0428+.078999t) - 12.80125 sin (.8975+.080511t) - 3.91667 sin (.2389+.083333t) - .83561 sin (.6269+.083561t) = 0.

Note that we have not expressed the angles in radians during the differentiation (as we should) because we are searching only for zeros. Once the time for the zero is found, say t₀, the corresponding height of high or low water is found by calculating z(t₀) in the preceding formula. One could also use Langrangian interpolation using equispaced values of z(t). The entire calculation can be done with the help of a handheld programmable calculator.

10. REFERENCES

- Anonymous. 1967. Tafeln der astronomischen Arguments $V_0 + v$ und der Korrekturen j, v . Deutsches Hydrographisches Institut. Hamburg. Nr. 2276: 128 p. (The nodal modulation f and u are denoted by j and v in this publication).
- Batchelor, B. G. 1972. Practical approach to pattern recognition. Plenum Press. xii + 243 p.
- Central Intelligence Agency. Cartographic Automatic Mapping (CAM). User's guide program documentation. Version 4, PB-238-358, December 1974. Prepared for Nat. Tech. Inf. Serv., IBM Federal Systems Div. Dist., U.S. Dep. Commerce, 111 p. (Miller projection p. 90. Devised by O.M. Miller, Am. Geogr. Soc. during WW II).
- Dawson, W. B. 1894. Report to the Engineer in Charge Tidal Survey. 1897. Character and progress of the tides in the Gulf and River St. Lawrence. Trans. R. Soc. Canada (2)3(3): 51-68. 1913. The tides of Hudson Bay. J. R. Astron. Soc. Canada. 8: 98-107. 1920. The tides and tidal streams with illustrative examples from Canadian waters. Dep. Naval Serv.: 1-43.
- Defant, A. 1961. Physical oceanography. Pergamon Press, Inc., New York, N.Y. 598 p. Part 2: Tides and tidal currents: 245-506.
- Dietrich, G. 1963. General oceanography. Interscience, John Wiley and Sons, New York, N.Y. xv + 588 p. (Contains cotidal charts of the world ocean).
- Dohler, G. 1964. Tides in Canadian waters. Can. Hydrogr. Serv., Mar. Sci. Br., Dep. Mines Tech. Surv. Ottawa, 14 p.
- Everett, J. D. 1879. Tides in the Bay of Fundy. Nature 19, 458.
- Farquharson, W. J. 1959. Report on tidal survey 1958. Investigation Northumberland Strait. Dep. Mines Tech. Surv. Ottawa, Surv. and Mapping Br. Ottawa, 137 p. 1962. Tides, tidal stations and currents in the Gulf of St. Lawrence. Can. Hydrogr. Inst. Mar. Sci. Br., Dep. Mines Tech. Surv. Ottawa, 76 p.
- Godin, G. 1972. The analysis of tides. Univ. Toronto Press. xxi + 264 p. 1976. The use of the admittance function for the reduction and interpretation of tidal records. Mar. Sci. Dir. MS Rep. 41: 46 p. 1977. The identification and classification of tidal records through pattern recognition. Mar. Sci. Dir. MS Rep. 42: 45 p. 1979. La marée dans le golfe et l'estuaire du Saint-Laurent. Naturaliste can. 106: 105-121.
- Godin, G., and J. Taylor. 1973. A simple method for the prediction of the time and height of high and low water. Intr. Hydrogr. Rev. 50(2): 75-81.
- Henry, R. F., and M. G. G. Foreman. 1977. Numerical model studies of semi-diurnal tides in the southern Beaufort Sea. Pac. Mar. Sci. Rep. 77-11, Inst. Ocean Sci. Patricia Bay, Victoria, B.C. (cotidal charts for the Beaufort Sea) 71 p.
- Redfield, A. C. 1950. The analysis of tidal phenomena in narrow embayments. Phys. Oceanogr. Meteorol. MIT and Woods Hole Oceanogr. Inst. 11(4): 36 p.
- Sterneck, R. 1922. Neue Weltkarten der Flutstundenlinien. Ann. Hydrog. Marit. Meteorol. 50: 145-149 (Berlin).

- Ward, J. O. 1970. User's guide to subroutine MAP. National Oceanogr. Data Center, April. (Description of Miller's projection).
- Whewell, W. 1833. Essay towards a first approximation to a map of cotidal lines. Phil. Trans. R. Soc. London, 147-236.

11. FIGURE CAPTIONS

Frontispiece. Place names in Canada on a Miller projection.

Fig. 1. Relation between the local constituent $A \cos (\sigma t - a)$ and the corresponding component of the tidal force $A' \cos V(t)$.

Fig. 2. Profile of the surface of a fluid in a canal and corresponding horizontal velocities at various times when it is disturbed by (a) a travelling wave and (b) a standing wave.

Fig. 3. Cotidal charts in a canal half a wavelength long (one-dimensional motion). Continuous line - cophase contour. Dashed line - coamplitude contour.

- a) Travelling wave: vertical displacement Z .
- b) Standing wave, no friction: vertical displacement Z and horizontal velocity u .
- c) Standing wave affected by friction: Z and u .

Fig. 4. Schematic cotidal charts for a standing Kelvin wave (no friction); they are the rotary counterpart of chart (b) in Fig. 3. The nodal line has been transformed into a point (amphidromy) by the rotation and the cophase lines now radiate from it. The node of the current (at X_1) corresponds to the antinode of the vertical displacement and vice versa.

Fig. 5. Cotidal chart of the vertical displacement Z for a standing Kelvin wave corresponding to the frequency of M_2 in a basin at latitude 45°N , width 200 km, depth 100 m, closed at $x = 0$ and of indefinite length. (a) Without friction. (b) With weak linearized friction, $r = 10^{-5}/\text{sec}$. (c) With moderate friction, $r = 5 \times 10^{-5}/\text{sec}$. (d) With strong friction, $r = 10^{-4}/\text{sec}$.

Fig. 6. Set of predicted levels for April 1978 at various stations to illustrate some actual tides corresponding to the indicated patterns. The stations chosen cover patterns from .4SD (almost pure semidiurnal) to 2.0D (almost pure diurnal). (a) .391 SD. Woods Harbour. Good semidiurnal tide with a slight diurnal inequality. (b) .483 SD. Halifax. Quite similar to Woods Harbour with a more marked diurnal inequality and more intense change from springs to neaps. (c) .608 SD. Rivière du Loup. Still a good semidiurnal tide with an even more marked change from springs to neaps. (d) 1.004 N. Holy Rood. We enter the normal category where the spectrum of the constituents is very similar to that of the tidal potential. (e) .195 M. Rivière au Renard. We enter the M (mixed) category where the diurnal portion of the spectrum of the constituents becomes larger than that in the tidal potential. The diurnal inequality is quite marked during the two semimensual maxima in the lunar declination which occur around hour 288 and hour 624 of the month. (f) .306 M. Pictou. (g) .501 M. Seattle, Washington, USA.

(h) .602 M. Lund. (i) .802 M. Gabriola Pass. (j) 1.003 D. Cowichan. We enter the D (diurnal) category where the probability increases that there will occur a single tide over a span of 24 hours. (k) 1.205 D. Saanichton Bay. (l) 1.401 D. Esquimalt. (m) 1.603 D. Caissie Point. This station lies to the southwest of the semidiurnal point of amphidromy which exists in Northumberland Strait. (n) 2.021 D. Gorge Victoria. Apparently the record with the most diurnal character available in our files. Both the diurnal and semidiurnal bands of the mixed tide entering from Victoria are damped while it propagates into the Gorge but the semidiurnal band is damped rapidly.

Fig. 7. Observed amplitude ratio and difference in the Greenwich phase lag between the pairs K_2 and S_2 , P_1 and K_1 . It is presented as a vector of length r (amplitude ratio) and inclined at an angle ϕ (difference of phase lag). These values are obtained at stations where the constituents are separable; they are used afterwards for inferring K_2 from S_2 and P_1 from K_1 at stations where they cannot be separated. Since the observed values depend on the geographical location, the measured vectors are presented in groups for the west coast, east coast and arctic. The tendency of the vector to bunch around a common value indicates that a mean value exists for the vector and the vector mean is presented in each case. The actually observed r , ϕ values are shown as rays in the larger diagram. Their vector average is shown in the smaller diagram as a single ray whose amplitude (\bar{r}) and orientation ($\bar{\phi}$, in degrees) are written out explicitly as "mean amplitude" and "mean angle".

Fig. 8. Cotidal charts for the constituents M_2 , S_2 , N_2 , K_1 and O_1 in waters adjacent to Canada. A Miller projection is used for the geographic background. The solid lines are contours of constant Greenwich phase lag; the dashed lines are contours of constant amplitude and the units degrees and centimeters. The contours are marked as 120° or 30 to indicate a Greenwich phase lag of 120° or a contour of 30 cm. The time zone used for all the maps is Greenwich ($Z = 0$). The spacing of the contours is not necessarily regular. Question marks indicate areas where it was not possible to conjecture the type of motion present either because of a shortage of data or of their poor quality. The signs + or - help visualize the direction of increasing or decreasing values in areas where this is not evident. (a) M_2 (b) S_2 (c) N_2 (d) K_1 (e) O_1 .

Fig. 9. Tide patterns in waters adjacent to Canada.

Fig. 10. Cotidal charts for the constituents M_2 , S_2 , N_2 , K_1 and O_1 in waters adjacent to the northern and southern portions of British Columbia. (a) M_2 (b) S_2 (c) N_2 (d) K_1 (e) O_1 .

Fig. 11. Patterns of the tide in waters adjacent to the northern and southern portions of British Columbia. (a) Northern portion. (b) Southern portion.

Fig. 12. Cotidal charts for the constituent M_2 , S_2 , N_2 , K_1 and O_1 around Newfoundland and off Cape Breton to the estuary of the St. Lawrence River. (a) M_2 (b) S_2 (c) N_2 (d) K_1 (e) O_1 .

Fig. 13. Cotidal charts for the constituent M_2 , S_2 , N_2 , K_1 and O_1 in the upper St. Lawrence River. (a) M_2 (b) S_2 (c) N_2 (d) K_1 (e) O_1 .

Fig. 14. Creation of a semimonthly tide in the upper reaches of the St. Lawrence River caused by the succession of spring and neap tides downstream (from Godin 1979).

Fig. 15. Tidal pattern around the Gulf of St. Lawrence and the upper estuary of the St. Lawrence River. (a) Gulf of St. Lawrence (b) Upper estuary.

Fig. 16. Cotidal charts for the constituents M_2 , S_2 , N_2 , K_1 and O_1 in the Bay of Fundy. (a) M_2 (b) S_2 (c) N_2 (d) K_1 (e) O_1 .

